Quantum Measurement Theory in Quantum Gravity

by

Benjamin Knepper

A bachelor's thesis submitted in partial satisfaction of the

requirements for the degree of

Bachelor of Arts (B.A.) with Honors

in

Physics

at the

University of California, Berkeley

Committee in charge:

Dr. Daniel Carney (Lawrence Berkeley National Laboratory), Advisor
Professor Luca Iliesiu (University of California, Berkeley), Co-advisor

Fall 2025

The bachelor's thesis of Benjamin Knepper, titled Quantum Measurement Theory in Quantum Gravity, is approved:

Advisor _____ Date _____

Co-advisor _____ Date _____

_____ Date _____

University of California, Berkeley

Quantum Measurement Theory in Quantum Gravity

Abstract

Quantum Measurement Theory in Quantum Gravity

by

Benjamin Knepper

in Physics

University of California, Berkeley

Dr. Daniel Carney (Lawrence Berkeley National Laboratory), Advisor

Professor Luca Iliesiu (University of California, Berkeley), Co-chair

Scientific progress depends on the precision and accuracy of measurements of nature that can be made. Quantum gravity is no exception. In this bachelor's thesis, we explore ways in which the theory of quantum measurements can be applied to observables in quantum gravity to help further elucidate the connection between these two pillars of 20th century physics.

In particular, we consider measuring two quantum gravity observables: the purity of Hawking radiation, and the length of a wormhole in JT gravity. Stephen Hawking infamously calculated that black holes destroy any information thrown into them. However, modern holographic theories of quantum gravity resolve this paradox by demonstrating that the information is not lost, but rather very "scrambled" in the radiation that black holes emit. Thus we investigate measurements which can probe the dynamical nature of this scrambling, which will be implemented on the Advanced Quantum Testbed (AQT) simulation platform. Moreover, a concrete holographic observable can be derived by considering the length of a wormhole in a 2D model of gravity. We discuss how to measure this length operator in the (nearly) dual Sachdev-Ye-Kitaev (SYK) system, considering both projective and continuous measurements in digital and analog quantum simulation platforms.

Developing measurements probing the information-theoretic structure of spacetime not only have the potential for generating experimental predictions that can be tested on near-term quantum simulators, but also provide a viable path for analyzing in-principle connections between general relativity and quantum mechanics. This thesis relied on a wide variety of tools and techniques, ranging from quantum optics to holography.

To my mom, Tory Herald.

Contents

List of Figures

Acknowledgments

I want to thank Dr. Daniel Carney for his incredible mentorship through this project over the past year, and for being willing to embark on this relatively unexplored topic with me. I have learned and benefited so much from our interactions, and with his guidance I am both ready and excited to pursue a lifelong career in this field.

I would also like to thank Professor Luca Iliesiu for serving as the co-advisor for this senior thesis, and for providing insightful feedback on the SYK measurement section through multiple Zoom meetings and in person discussions.

Much of the technical work of this thesis has been performed in collaboration with Lawrence Berkeley Laboratory postdoc Manthos Karydas, for whom I am grateful for sustained discussions for hours in the LBNL office or at conferences and talks.

I am also grateful to Professor Julian Sonner at the University of Geneva for collaboration on the SYK measurements topic and helpful technical guidance on many of the holography components.

I also thank professor Geoff Penington for initially serving as my senior thesis co-advisor.

Chapter 1

Quantum Measurement of Hawking Radiation Purity

1.1 Measuring Hawking radiation at late times

Stephen Hawking infamously calculated that black holes destroy information. Specifically, he conjectured that the dynamics of black hole evaporation could in principle turn the initial state of a black hole formed by the collapse of a star with microscopic structure entirely into thermal radiation, thereby converting a pure stated into a mixed state and violating the unitarity of time evolution in quantum mechanics [43].

Much progress has been made by considering the quantum-information theoretic aspects of black holes more closely. In particular, tools from quantum computing have proven lucrative for making models which help show how the "black hole information paradox" can be resolved. Broadly speaking, many quantum information theoretic models frame the process of black hole evaporation in the language of subsystems: we treat the Hawking radiation and black hole microstates as two subsystems with states ρ_B and ρ_R, which are highly entangled (see figure 1.1).

The islands developments in AdS/CFT [69, 3] have corroborated the unitarity of black hole evaporation, which leads to a testable hypothesis: a measurement post-evaporation

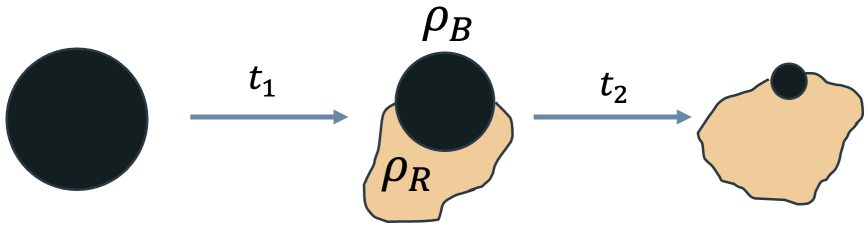

Figure 1.1: Quantum information-theoretic cartoon of black hole evaporation process.

should confirm that Hawking radiation is in a pure, not mixed, state. We ask the question: what is the most efficient measurement that one could perform to determine the purity of Hawking radiation subsystem?

The most brute force approach is to perform full-state tomography of ρ_R. It is a suprising and powerful fact in quantum metrology that a global density matrix of a many-body system can be reconstructed to sufficient precision by performing local measurements. This result is encapsulated in the following axiom [15]:

> **Axiom of Local Tomography:** For any quantum state ρ in a Hilbert space $\mathcal{H} = \mathcal{H}_1 \otimes \mathcal{H}_2 \otimes \ldots$, there exists a set of local measurements on subsystems $\mathcal{H}_i$ which can reconstruct $\tilde{\rho}$ to a sufficient accuracy $\|\rho - \tilde{\rho}\| \leq \varepsilon$.

State tomography is a procedure which reconstructs an unknown density matrix by performing measurements on multiple copies of that state. For a many-body system in a Hilbert space of dimension $d = 2^N$, a general representation for any density matrix in the compu-tataional basis will be

$$\rho = \frac{1}{d} \sum_{i=1}^{d^2} p_i \Sigma_i \tag{1.1}$$

where Σ_i are Pauli strings of length N. The point of state tomography is to determine the weights

$$p_i = \mathrm{Tr}(\rho \Sigma_i) \tag{1.2}$$

which can be done by performing multiple generalized measurements with POVMs

$$E_i = \frac{1 \pm \Sigma_i}{2} \tag{1.3}$$

on d^2 copies of ρ [15]. After reconstructing $\tilde{\rho}$ through these measurements, we can then compute the purity of ρ via $\mathrm{Tr}(\tilde{\rho}^2)$.

In general, the reconstruction error goes as $\varepsilon = \left(\frac{1}{\sqrt{M}}\right) d$. So for an error of 0.01, we would need to perform $10^4 \cdot 2^{2N}$ measurements, which quickly becomes computationally expensive. Thus we are led to ask, can we come up with a more efficient measurement scheme to distinguish scrambling from thermalization and verify the purity of Hawking radiation?

The procedure for determining purity from state tomography outlined above does not leverage entanglement in the measurements. In general, more efficient entangled-measurement schemes have been developed for performing purity measurements. In practice, this means that the measurement algorithm involves "quantum memory" by storing the measurement outcomes in ancillas or other systems so that they can be correlated as opposed to taking multiple independent measurements.

For example, it was shown in [17] that if one uses a version tomography known as "shadow tomography" with quantum memory leveraging k ancillas, then to distinguish between a pure and maximally mixed state one would only need to use $C = O(2^{(n-k)/3})$ copies as opposed to the $C = O(2^{n/2})$ copies required without quantum memory.

An entangled-measurement scheme which is perhaps the most straight-forward way to measure purity is the SWAP test. It uses the SWAP gate, which acts on a two-body Hilbert space and swaps the order of two quantum states,

$$\text{SWAP}\,|i\rangle\,|j\rangle = |j\rangle\,|i\rangle\,. \tag{1.4}$$

Given just two copies of a quantum state $\rho = \sum_i p_i\,|v_i\rangle\langle v_i|$, the SWAP operator acting on the combined state $\rho^{\otimes 2}$ yields the purity as its expectation value [11]:

$$\begin{aligned}
\text{Tr}\big(\text{SWAP}\rho^{\otimes 2}\big) &= \sum_{i,j} p_i p_j\,\text{Tr}(\text{SWAP}\,|v_i\rangle\langle v_i| \otimes |v_j\rangle\langle v_j|) \\
&= \sum_{i,j} p_i p_j\,\text{Tr}(|v_j\rangle\langle v_i| \otimes |v_i\rangle\langle v_j|) \\
&= \sum_{i,j} p_i p_j |\,\langle v_i|v_j\rangle\,|^2 \\
&= \sum_i p_i^2 \\
&= \text{Tr}\big(\rho^2\big)
\end{aligned} \tag{1.5}$$

This SWAP test also naturally extends up to higher dimensional many-body systems [19]. In the context of holography, a bulk and boundary interpretation of this SWAP operator has been discussed in [26] and [27].

While these measurements ensure greater efficiency over full local tomography, we can ask a further question. Instead of performing a measurement post-evaporation, is there a measurement protocol that one could perform to detect the dynamics of purification as opposed to thermalization in black holes?

1.2 OTOC Measurements of the Page Curve

By considering random pure states, Don Page was able to construct an argument for how information could be retrieved in the Hawking radiation of an evaporating black hole [68]. He modeled the full system as being in a random pure state, and considered the dynamics of entanglement entropy of the radiation subsystem. In particular, he showed that as time increases, the Von Neumann entropy $S_R = -\,\text{Tr}(\rho_R \log(\rho_R)))$ initially increases in line with Hawking's thermal prediction. However, when the subsystem size of the radiation and the black hole microstates become the same value of $N/2$, where N is the total number of degrees of freedom, there will be a phase transition. This turning point is known as the Page time t_{Page}, after which the entanglement entropy of the radiation subsystem will start to decrease, eventually reaching zero at the end of the evaporation process when its subsystem size is N. Therefore, the state ρ_R will be pure again at the end of the evaporation process, in contrast to Hawking's original prediction that the entanglement entropy monotonically increases. See figure 1.2 for a diagram of the Page curve.

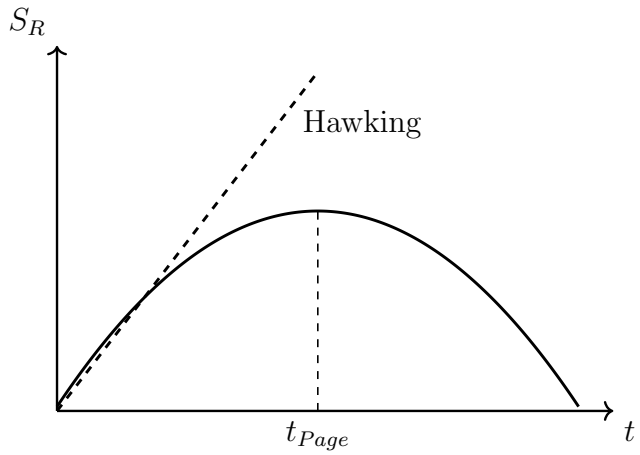

Figure 1.2: Page Curve

Let L be the size of the radiation subsystem. The Von Neumann entropy of the radiation subsystem over all random pure states in the regime where $L \gg 1$ is [68]

$$S_R^{VN} \approx L\log(2) - \left(\frac{1}{2^{N-2L-1}}\right). \tag{1.6}$$

For any density matrix ρ, the most general form of entanglement entropies are the Renyi-α entropies defined by

$$S^{(\alpha)}(\rho) = \frac{1}{1-\alpha}\log(\mathrm{Tr}(\rho^\alpha)). \tag{1.7}$$

The limit $\alpha \to 1$ recovers the familiar von Neumann entropy $S^{(1)} = -\mathrm{Tr}(\rho\log(\rho))$ [58]. The second Renyi entropy is also interesting to consider as it directly probes the purity: $S^{(2)}(\rho) = -\log(\mathrm{Tr}(\rho^2))$.

Returning to the Page curve, the average second Renyi entropy for the radiation subsystem over all pure states is

$$S_R^{(2)} = -\log\left(\frac{2^L + 2^{N-L}}{2^N + 1}\right). \tag{1.8}$$

This shows that the von Neumann entropy used in the Page curve is an upper bound of the corresponding Renyi entropy of the radiation subsystem, which we will use in our subsequent analysis of purity measurements [19].

Indeed, black holes are thought to be among the most chaotic systems in nature. They exhibit dynamics known as "quantum information scrambling," whereby local degrees of freedom in ρ_R are delocalized across the whole Hilbert space due to highly entangled interactions [88]. In fact, black holes are considered "fast scramblers," meaning the time at which degrees of freedom can no longer be recovered from local probes saturates the fastest time of delocalization known as the scrambling time t_* [78, 53],

$$t_* \approx \log(N) \tag{1.9}$$

for N degrees of freedom. Other systems which can saturate this timescale are Haar-random unitary circuits, similar to the setup proposed by Page [9, 14]. As such, much progress has been made modeling black hole evaporation with Haar-random unitaries.

How can we effectively use a quantum computer to study the Page curve dynamics? There are two main usages: the first is to have an observer stationed outside of the black hole, collecting Hawking quanta as they fall out and measuring the entanglement entropy of the radiation in a quantum computer. This is essentially the approach of Hayden-Preskill, who showed that after the Page time there is a decoding protocol that one can perform on the radiation states that can almost immediately recover the an initial state thrown into the black hole [44, 90]. In this case, the time evolution of the Page curve is governed by the genuine evaporation time evolution of the black hole.

The second is to use the quantum system to simulate the evaporation dynamics. In this approach, the time evolution is replaced by sufficiently random or chaotic unitary gates, which resemble fast scrambling. The "time-evolution" of the evaporation dynamics is then modeled by considering increasing subsystem size after the scrambling unitary is applied to the full system. In particular, a subsystem of $N/2$ qubits would correspond to the stage of the evaporation at t_{Page}. This is the approach we will take below.

Moreover, in chaotic and thermalizing systems, a useful correlator has been developed which can quantify quantum information scrambling known as the Out-of-Time-Ordered-Correlator (OTOC) F_t [88, 83, 31, 90]. The OTOC is a four point correlator between two local operators W, V which diagnoses the failure of these two operators to commute, thereby indicating operator spreading and scrambling. The OTOC takes the form

$$F_t = \left\langle W^\dagger(t) V^\dagger W(t) V \right\rangle . \tag{1.10}$$

In most cases we will choose W and V to be unitary and Hermitian. In doing so, the OTOC has a natural interpretation of diagnosing scrambling and chaos from the butterfly effect picture: it computes the overlap of the states $W(t)V\left|\psi_0\right\rangle$ and $VW(t)\left|\psi_0\right\rangle$. In the former, we start in some initial state, act with V, time evolve, perturb with W and then evolve backwards in time. In the latter, we switch the order of operations, first evolving in time, perturbing with W, evolving backwards in time, and then acting with V. For integrable and near equilibrium systems, these two orders of operations will produce the same effect; the OTOC will be approximately 1. For chaotic systems, by contrast, even a small perturbation at late times or a slight difference in intial conditions will result in vastly different final conditions; the OTOC will exponentially fall to 0.

We can also consider the squared commutator

$$C_t = \left\langle [W(t), V]^2 \right\rangle . \tag{1.11}$$

which probes operator spreading growth. After expanding, the OTOC is related to this squared commutator by

$$C_t = 2(1 - F_t). \tag{1.12}$$

Measurement protocol

Instead of measuring the purity of the radiation post-evaporation, we consider now constructing a measurement protocol to observe Page curve dynamics in the radiation subsystem. Given that OTOCs are operators which quantify the progression of chaos over time, it is natural to wonder whether they can be used to probe the increase and decrease of Renyi entropy (RE) $S_R^{(2)}$.

For an initial mixed state, there is an OTOC-RE relation that was discovered in [46, 29] and subsequently discussed in [92], which we now review as it provides relevant insight the case of an initial pure state as in the black hole evaporation setup. Consider two complementary subsystems A, B. Then the OTOC-RE theorem states

$$e^{-S_A^{(2)}} = \frac{1}{d_B} \int d\hat{V} \left\langle \hat{W}_B(t) \hat{V} \hat{W}_B(t) \hat{V} \right\rangle_{\beta=0} \tag{1.13}$$

where the expectation value is over a thermal Gibbs state of inverse temperature β. Here we are assuming that both $\hat{W}_B$ and $\hat{V}$ are Hermitian and unitary, and $\hat{W}_B$ acts only on the subsystem B. Equation (1.13) shows that by acting with operators on subsystem B, one can determine the purity $\mathrm{Tr}(\rho_A^2) = e^{-S_A^{(2)}}$ of subsystem A. This theorem can also be naturally extended to finite temperature systems with Euclidean insertions of $e^{-\beta H}$ in the correlator.

In our case, we assume the black hole starts in a pure state, $\rho(t=0) = |\psi_0\rangle\langle\psi_0|$. As such, we can draw from the quantum metrology literature and consider a variant of the OTOC known as the Fidelity OTOC (FOTOC) in which the operators are chosen such that $V = |\psi_0\rangle\langle\psi_0|$, $W = e^{i\theta G}$ where G is some Hermitian generator of the unitary transformation. With this prescription, the OTOC becomes a fidelity measurement

$$F_t = \mathrm{Tr}(\rho_0 \rho_t(\theta)) \tag{1.14}$$

where $\rho_t(\theta) \equiv e^{-i\theta G} e^{iHt} \rho_0 e^{-iHt} e^{i\theta G}$ [33].

We can take inspiration from the OTOC-RE theorem above and try to adapt it for the case of the FOTOC to probe the Renyi entropy of the radiation subsystem ρ_R. Indeed an analog exists and is alluded to in [54]. Specifically, an arbitrary density matrix ρ can be decomposed into blocks called multiple quantum coherences (MQCs) given by

$$\rho = \sum_m \sum_{\lambda_i - \lambda_j} \rho_{ij} |\psi_i\rangle\langle\psi_j| = \sum_m \rho_m \tag{1.15}$$

where ρ_m encodes all the coherences between quantum states with eigenvalues λ_i of some operator G which differ by m. The coherences of these blocks can be quantified with the norm

$$I_m = \mathrm{Tr}\big(\rho_m^\dagger \rho_m\big) = \mathrm{Tr}(\rho_{-m}\rho_m). \tag{1.16}$$

In particular, from (1.14), the FOTOC can be written as the Fourier transform of these multiple quantum coherences [33]

$$F_t = \sum_m I_m \rho_m(t) e^{im\theta}. \tag{1.17}$$

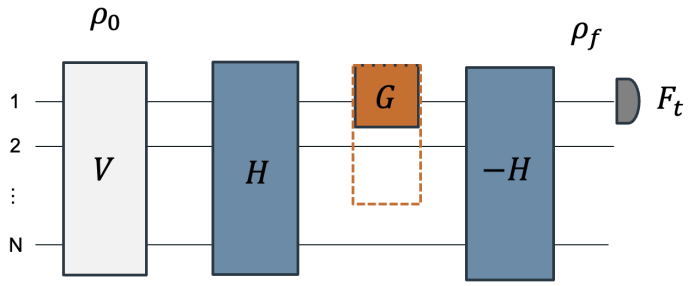

Figure 1.3: Quantum circuit diagram schematic for OTOC measurement of Page curve.

As such, one can experimentally determine the weights I_m by measurements of the FOTOC at various times.

Similar to the OTOC-RE theorem above, the authors in [54] show that the Renyi entropy of a subsystem determined by the support of the operator G which generates the unitary $W(\theta)$ can be determined by these multiple quantum coherence weights:

$$S^{(2)}(\rho_G) = -\log\left(I^G_{m=0} + I^{G^c}_{m=0}\right) \tag{1.18}$$

where I^G corresponds to multiple quantum coherences on the G subsystem, and I^{Gc} to coherences on the G^c subsystem. The $m = 0$ mode is important because in this case the coherence norms give the purity $I_{m=0} = \mathrm{Tr}(\rho^2_{m=0})$, which can be approximated by performing measurements over a full range of angles θ.

Thus by taking the OTOC measurement at various times, from which the weights I_m are obtained by inverse Fourier transforming, one can determine the second Renyi entropy, and therefore the purity, of a subsystem. Here, we treat the subsystem that G acts on as the radiation subsystem and the complement as the black hole subsystem. We can model the effect of measurements at different times by varying the support of the generator G across the quantum circuit as shown in figure 1.3. When G has support on $N/2$ qubits, we expect to see the Page phase transition and thus in performing multiple measurements near this regime will be able to diagnose the expected purification effect for models of black hole evaporation. While this protocol achieves a probe of subsystem entropy through OTOC measurements, it requires global control through measurements also on the complement subsystem G^c, which in the black hole evaporation language is ρ_B. Given that the black hole interior should be inaccessible to local measurements, in ongoing work we are investigating information-theoretic ways to remedy this effect and modify the protocol to only depend on G subsystem measurements.

1.3 Pseudorandom Scrambling Simulation at the Advanced Quantum Testbed (AQT)

Leveraging recent advances in quantum simulation, we are in an era where one can actually implement such models of black hole evaporation on quantum computing platforms. Following the procedure above, there are two essential experimental simulation tasks: 1) identify a scrambling unitary U_s to implement the time evolution, and 2) measure the OTOC.

Many quantum circuit models of information scrambling have been developed [88], and among them the ideal models for simulating black hole evaporation would be "fast scrambling." As explained by Belyansky et al. [7], a minimal model for fast scrambling requires a generating Hamiltonian with a local H_I and global H_{II} term, $H = H_I + H_{II}$. One common variant of this model is to trotterize the local and global components into alternating circuit layers, so that the scrambling unitary at time t becomes $U(t) = (U_I U_{II})^t$. For example, the authors of [7] demonstrate that

$$U_I = \prod_{i=1}^{N} U_{H,i} \tag{1.19}$$

$$U_{II} = \exp\Big(-\frac{g}{\sqrt{N}} \sum_{i<j} Z_i Z_j\Big), \tag{1.20}$$

with U_I being single-site Haar-random unitaries and U_{II} a global chaotic spin chain, is sufficient to achieve a fast scrambling time of $t_* \propto \log(N)$.

However, on real (digital) quantum simulation platforms, the global couplings of the form U_{II} are experimentally challenging to implement. Instead, one can attempt to be clever by reducing the size of the couplings in U_{II} while increasing the size of the Hilbert space dimension. This was the approach that the Lawrence Berkeley National Laboratory Advanced Quantum Testbed (AQT) took in [10], by implementing quantum information scrambling on three-level-system superconducting qutrits, using a teleportation algorithm developed by Yoshida and Yao [91]. The scaling of of subsystem size in qu*d*its enables complex simulation tasks on fewer devices. As a concrete example, the Hilbert space dimension of two qutrits is greater than that of three qubits. In superconducting transmons, the anharmonicity of the Josephson junction potential enables the experimental realization of subspaces greater than 2 [84, 37, 66].

Moreover, not only does pseudorandomness provide a viable tool for modeling scrambling given the previous work by Hayden-Preskill and Page on black hole information dynamics, but also elucidating the connections between randomness, quantum chaos, and scrambling is an active area of research [9, 58, 38]. Therefore, as part of this senior thesis, we proposed to extend this previous AQT work and perform a quantum information scrambling simulation on pseudorandom qutrit gates.

We took inspiration from [65] where random diagonal unitaries are used to generate many-body localization and discrete time-crystalline phases. Given that in our case we want

to simulate disordered as opposed to ordered phases, we implement the brickwork layer approach above and in [64], by interweaving layers of single-site random unitaries U_I as in (1.19) and U_{II} given by

$$U_{II}(\theta_{22},\theta_{23},\theta_{32},\theta_{33}) = \mathrm{diag}(1,1,1,1,e^{i\theta_{22}},e^{i\theta_{23}},1,e^{i\theta_{23}},e^{i\theta_{33}}) \tag{1.21}$$

as represented in the computational basis. The angles couple the subspaces 2 and 3 between two neighboring qutrits, and are randomly sampled from $\theta_i \in [-3\pi/2, \pi/2]$. The local "Haar" gates U_I can be constructed from Cliffords, which in reality form a 2-design [75]. Again, the full scrambling unitary becomes $U_s(t) = (U_I U_{II})^t$.

Before discussing numerical simulations of this pseudorandom qutrit scrambling unitary, we can attempt to analytically quantify its closeness to Haar-randomness using the techniques from unitary k-designs, which we now review.

When integrating observables over the Haar measure, we can use the identities

$$\int_{\mathrm{Haar}} dU = 1, \quad \int_{\mathrm{Haar}} dU f(U) = \int_{\mathrm{Haar}} dU f(UV) = \int_{\mathrm{Haar}} dU f(VU) \tag{1.22}$$

for $V \in U(H)$. Oftentimes, one is interested in developing an ensemble of unitaries which resemble the Haar ensemble up to some number of moments. For any arbitrary ensemble, we can define the k-fold channel as

$$\Phi_{\mathcal{E}}^{(k)}(A) = \int_{\mathcal{E}} dA (U^{\otimes k})^\dagger A U^{\otimes k} \tag{1.23}$$

which encapsulates the effect of transforming an operator under k moments of unitaries drawn from the ensemble. For the case of a Haar ensemble, (1.23) recovers the familiar rule for Haar conjugation in the special case of $k = 1$ and dimension d:

$$\int_{\mathrm{Haar}} dU U^\dagger A U = \frac{1}{d}\,\mathrm{Tr}(A). \tag{1.24}$$

It is a theorem that an ensemble is a unitary k-design if an only if

$$\Phi_{\mathcal{E}}^{(k)}(A) = \Phi_{\mathrm{Haar}}^{(k)}(A). \tag{1.25}$$

However, there also exists a more streamlined test of k-design known as the *frame potential*,

$$\mathcal{F}_{\mathcal{E}}^{(k)} = \int_{U,V\in\mathcal{E}} dU dV |\,\mathrm{Tr}\big(U^\dagger V\big)|^{2k}. \tag{1.26}$$

For a Haar-random ensemble, $\mathcal{F}_{\mathrm{Haar}}^{(k)} = k!$. Frame potentials provide a more computationally direct way of quantifying how Haar-random a unitary ensemble is through the following theorem:

$$\mathcal{F}_{\mathcal{E}}^{(k)} \geq \mathcal{F}_{\mathrm{Haar}}^{(k)}, \tag{1.27}$$

with equality if and only if $\mathcal{E}$ is a k-design [21, 75].

We can use these k-design techniques to help us quantify the ranndom scrambling unitaries that we defined above. In this case, the ensemble is given by $\mathcal{E} = \{U_s\}$. Then for N qubits, its frame potential is given by

$$\begin{aligned}
\mathcal{F}_{\mathcal{E}}^{(k)} &= \iint_{U_s,V_s\in\mathcal{E}} dU_s dV_s |\operatorname{Tr}\big(U_s^\dagger V_s\big)|^{2k} \\
&= \int_{\substack{U_I,V_I\in\text{Haar},\\ \bar\theta\in[-3\pi/2,\pi/2]}} dU_I dV_I dU_{II} dV_{II} \Big|\operatorname{Tr}\Big(U_{II}^\dagger(\bar\theta) U_I^\dagger V_I V_{II}(\bar\theta)\Big)\Big|^{2k} \\
&= \int_{\substack{V_I\in\text{Haar},\\ \bar\theta\in[-3\pi/2,\pi/2]}} dV_I dU_{II} dV_{II} \Big|\operatorname{Tr}\Big(U_{II}^\dagger(\bar\theta) V_{II}(\bar\theta) V_I\Big)\Big|^{2k} \\
&= \underbrace{\int_{\bar\theta\in[-3\pi/2,\pi/2]} dU_{II} dV_{II} \Big|\operatorname{Tr}\Big(U_{II}^\dagger(\bar\theta) V_{II}(\bar\theta)\Big)\Big|^{2k}}_{(\mathcal{F}_{II}^{(k)})} \underbrace{\int_{V_I\in\text{Haar}} dV_I \Big|\operatorname{Tr}(V_I)\Big|^{2k}}_{(\mathcal{F}_{I}^{(k)})}
\end{aligned} \tag{1.28}$$

In the third line we used (1.22). In the fourth line, we used the fact that the $\bar\theta$ are drawn independently and the Haar measure separates ensemble averages. Evaluating the two integrals above [62],

$$\mathcal{F}_I^{(k)} = \int_{V_I\in\text{Haar}} dV_I \operatorname{Tr}(V_I)^k \operatorname{Tr}\Big(V_I^\dagger\Big)^k = \operatorname{Tr}\left(\int_{V_I\in\text{Haar}} dV_I (V_I^{\otimes k})^\dagger V_I^{\otimes k}\right) = |S_k| = k! \tag{1.29}$$

which is just the Haar frame potential. Using (1.21) and $k = 1$, the first integral reduces to

$$\mathcal{F}_{II}^{(1)} = \int_{-3\pi/2}^{\pi/2} d\bar\theta d\bar\theta' \Big|5 + \sum_{i\in\{22,23,32,33\}} e^{i(\theta_i - \theta_i')}\Big|^2. \tag{1.30}$$

For $k = 1$ and normalizing the integral above, we get $\mathcal{F}_{II}^{(1)} = 29$ meaning that

$$\mathcal{F}_{\mathcal{E}}^{(1)} = 29\mathcal{F}_{\text{Haar}}^{(1)}. \tag{1.31}$$

Therefore, this ensemble $\mathcal{E}$ only forms an approximate 1-design so we do not expect for it to achieve fast scrambling, in line with the fact that we have chosen U_{II} to couple nearest neighbor qutrits for experimental feasibility as opposed to the global coupling required for minimal fast scrambling models. Nonetheless, we can still quantify relevant scrambling rates and Lieb-Robinson bounds with this ensemble.

The most brute force way to measure the OTOC is to implement a circuit which exactly reconstructs $F_t = VU_sWU_s^\dagger V^\dagger U_s W^\dagger U_s^\dagger$ piece by piece, then performs a fidelity measurement. This method gives the amplitude squared $|F_t|^2$ without keeping track of any phase information in the correlator, yet nonetheless provides a simple test to observe general scrambling dynamics which should decay the four point correlator.

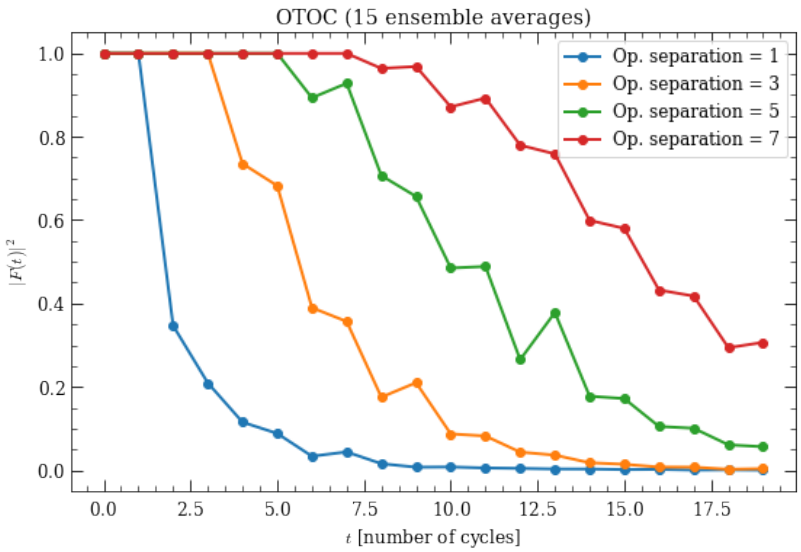

Figure 1.4: Google Cirq simulation exhibiting OTOC decay on qutrits for $U_s = U_I U_{II}$

We have manually coded a qutrit Google Cirq module to implement an OTOC scrambling circuit with $U_s = U_I U_{II}$ as defined above. Figure 1.4 shows the results for $V = X$ fixed on qutrit one and $W = Z$ on qutrits of varying operator separation distances. The plot exhibits the expected decay of the OTOC from information scrambling. It also confirms this rate of decay decreases as the operator separation between W and V increases, allowing more time to traverse before the commutator $[W(t), V]$ becomes nonzero.

There are more efficient ways to measure the OTOC beyond the brute force method discussed above [81, 89, 51]. One promising method for the digital qutrit platform is known as the "interferometric protocol" which utilizes an ancilla qubit C prepared in the state $|+\rangle_C = \frac{1}{\sqrt{2}}(|0\rangle_C + |1\rangle_C)$. In this protocol, the components of the OTOC are then separately applied to the system A and the ancilla, allowing the circuit depth to be cut in half. The final state generated is

$$|\Psi(t)\rangle = \frac{(VW(t)\,|\psi(0)\rangle)_A \otimes |0\rangle_C + (W(t)V\,|\psi(0)\rangle)_A \otimes |1\rangle_C}{\sqrt{2}} \tag{1.32}$$

via the following algorithm taken from [81]:

1. $\mathbb{1}_A \otimes |0\rangle\langle 0|_C + V_A \otimes |1\rangle\langle 1|_C$
2. $U_s(t)_A \otimes \mathbb{1}_C$
3. $W_A \otimes \mathbb{I}_C$
4. $U_s(-t)_A \otimes \mathbb{1}_C$.
5. $V_A\,|0\rangle\langle 0|_C + \mathbb{1}_A \otimes |1\rangle\langle 1|_C$.

Then the real and imaginary parts of the OTOC are given by X and Y measurements on the control qubit,

$$F_t = \langle X \rangle_C + i \langle Y \rangle_C \tag{1.33}$$

We are in the process of simulating this more efficient OTOC measurement protocol on the qutrit pseudorandom unitary U_s, in preparation for an experiment at the AQT in 2026.

Chapter 2

Quantum Measurements of Wormhole Length

This chapter is based on work to appear in collaboration with Manthos Karydas (LBNL), Daniel Carney (LBNL), and Julian Sonner (University of Geneva) titled "Quantum Measurement Theory of Holographic Wormhole Length" (2026).

2.1 JT Gravity Wormhole Length

Identifying and characterizing measurable observables in quantum gravity has been an important initiative for high energy theory across a wide range of sub-fields [72, 34, 42, 16]. In this portion of my senior thesis, we investigated the measurement-theoretic properties of one such quantum gravity observable—the length of a wormhole in a two-dimensional model known as Jackiw-Teitelboim (JT) gravity [48, 82]. We first review the basics of JT gravity and the derivation of this length operator by Harlow and Jafferis [41].

JT Gravity Review

JT gravity is a particular example of a 2D "dilaton" gravity model [28]. Dilaton models modify the Einstein-Hilbert action by coupling the Ricci scalar R to a new scalar field Φ, the dilaton,

$$S = \frac{1}{16\pi G_N}\int d^2x\sqrt{-g}R + \cdots \longrightarrow \frac{1}{16\pi G_N}\int d^2x\sqrt{-g}\Phi R + \ldots \tag{2.1}$$

and in general 2D dilaton gravity models include a dilaton potential parametrized by a single function $U(\Phi)$. For JT gravity, $U(\Phi) = -\Lambda$, where Λ is the cosmological constant. In the case of AdS2, one sets $\Lambda = -2/l^2_{\text{AdS}}$. After including the other topolological Einstein-Hilbert

terms, the full action for nearly AdS_2 classical JT gravity takes the form

$$S = \frac{1}{16\pi G_N}\Big[\Phi_0\left(\int_M d^2x\sqrt{-g}R + 2\int_{\partial M} dt\sqrt{|\gamma|}K\right) + \int_M d^2x\sqrt{-g}\Phi\Big(R + \frac{2}{l^2_{\text{AdS}}}\Big) \\ +2\int_{\partial M} dt\sqrt{|\gamma|}\Phi(K - \frac{1}{l_{\text{AdS}}})\Big]\,, \tag{2.2}$$

where K is the extrinsic curvature and $\gamma_{\mu\nu}$ is the induced boundary metric [41]. JT gravity has provided wide applications to studying near-extremal black holes and the information paradox [28].

In more detail, the solutions to the equations of motion are described by pieces of AdS_2 given by

$$ds^2 = -dT_1^2 - dT_2^2 + dX^2\,, \tag{2.3}$$
$$T_1^2 + T_2^2 - X^2 = l^2_{\text{AdS}}. \tag{2.4}$$

The AdS_2 solution in "Schwarzschild coordinates" is given by

$$\begin{aligned} T_1 &= l_{\text{AdS}}(r/r_s) \\ T_2 &= l_{\text{AdS}}\sqrt{(r/r_s)^2 - 1}\sinh\big(tr_s/l^2_{\text{AdS}}\big) \\ X &= l_{\text{AdS}}\sqrt{(r/r_s)^2 - 1}\cosh\big(tr_s/l^2_{\text{AdS}}\big) \end{aligned} \tag{2.5}$$

which one can check satisfies (2.4). Here r_s is the Schwarzschild radius.

In Schwarzschild coordinates, the metric and dilaton take the form

$$ds^2 = -\frac{r^2 - r_s^2}{l^2_{\text{AdS}}}dt^2 + \frac{l^2_{\text{AdS}}}{r^2 - r_s^2}dr^2 \tag{2.6}$$
$$\Phi = \Phi_h\frac{r}{r_s} = \Phi_h\frac{T_1}{l_{\text{AdS}}} \tag{2.7}$$

where $\Phi|_{r=r_s} = \Phi_h$ is the value of the dilaton on the horizon. Therefore, we take Φ_h to be dimensionless, and T_1 to have units of length.

By setting $r = r_c \to \infty$ to be the cutoff radius, we can derive the boundary conditions,

$$\gamma_{tt}|_{\partial M} = -\frac{r_c^2}{l^2_{\text{AdS}}}\,, \tag{2.8}$$
$$\Phi|_{\partial M} = \Phi_h\frac{r_c}{r_s} = \frac{\phi_b}{l^2_{\text{AdS}}}r_c \tag{2.9}$$

where γ is the induced metric on ∂M and we have defined the boundary dilaton as the characteristic length scale

$$\phi_b = \frac{l^2_{\text{AdS}}\Phi_h}{r_s}. \tag{2.10}$$

As we will show, the dilaton parameters Φ_h and ϕ_b provide the relevant parametrizations of the renormalized geodesic length L (i.e. wormhole length) and bulk wavefunctions Ψ.

Additionally, the AdS_2 solution in "global coordinates" is given by [39]

$$T_1 = \sqrt{l_{\text{AdS}}^2 + x^2}\cos(\tau/l_{\text{AdS}}) \tag{2.11}$$

$$T_2 = \sqrt{l_{\text{AdS}}^2 + x^2}\sin(\tau/l_{\text{AdS}}) \tag{2.12}$$

$$X = x \tag{2.13}$$

which using (2.3) yields

$$ds^2 = -\frac{l_{\text{AdS}}^2 + x^2}{l_{\text{AdS}}^2}d\tau^2 + \frac{l_{\text{AdS}}^2}{l_{\text{AdS}}^2 + x^2}dx^2 \tag{2.14}$$

$$\Phi = \Phi_h\sqrt{1 + (x/l_{\text{AdS}})^2}\cos(\tau/l_{\text{AdS}}). \tag{2.15}$$

We can relate the global time τ to Schwarzschild times $t = t_L$ or $t = t_R$ on either the left or right boundary of the 2D model via

$$\cos(\tau/l_{\text{AdS}}) = \frac{1}{\cosh(r_s t_L/l_{\text{AdS}}^2)} = \frac{1}{\cosh(r_s t_R/l_{\text{AdS}}^2)}. \tag{2.16}$$

Also worth noting here is the so-called "semi-classical" limit convention for JT gravity, following [41]. Equation (2.9) resembles the conventional dilaton boundary conditions [63, 2, 28],

$$\Phi|_{\partial M} = \frac{a}{\epsilon} + (\text{subleading as } \epsilon \to 0), \tag{2.17}$$

if we identify $\epsilon = l_{\text{AdS}}^2/r_c$ as the "near boundary cutoff" and $\phi_b = a > 0$ as the boundary dilaton length. Then the Schwarzian JT action becomes

$$S_{\text{grav}} = -\frac{\phi_b}{8\pi G_N}\int dt\{f(t), t\}\,, \tag{2.18}$$

where $\{f(t), t\} = f'''/f' - \frac{3}{2}\left(f''/f'\right)^2$ thus $\int dt\{f(t), t\}$ has dimension $(\text{length})^{-1}$ [63]. To get intuition for the JT semi-classical limit and as a preview for the nearly dual correspondence between JT gravity and a chaotic many-body system called the Sachdev-Ye-Kitaev (SYK) Model, let us for a moment consider the SYK Schwarzian action which has the form

$$S \sim \frac{N}{J}\sum_i \int dt\{f_i(t), t\} \tag{2.19}$$

where J is the SYK coupling. Matching the bulk and boundary Schwarzian actions, we see that

$$\frac{\phi_b}{G_N} \sim \frac{N}{J} \tag{2.20}$$

so sending $G_N \to 0$ or $N \to \infty$ has the same effect as $\phi_b \to \infty$. In pure AdS, we therefore expect the semi-classical limit is $\phi_b/l_{\text{AdS}} \gg 1$; in thermally excited AdS with inverse temperature β, it is when $\phi_b/(G_N\beta) \gg 1$.

Length Operator in JT Gravity

Now we provide the derivation for the quantum operator corresponding to the length of a wormhole in JT gravity following [41]:

$$L = 2l_{\text{AdS}} \ln\left(\frac{\cosh\left(\sqrt{\frac{8\pi G_N E}{\phi_b}}\delta\right)}{\sqrt{8\pi G_N \phi_b E}}\right). \tag{2.21}$$

where δ is the canonical time coordinate and E is the combined boundary energies.

We begin by defining the JT Hamiltonian via the boundary stress energy tensor. If we define a boundary "CFT metric" as

$$\gamma_{\mu\nu}^{\text{CFT}} = \frac{l_{\text{AdS}}^2}{r_c^2}\gamma_{\mu\nu}\,, \tag{2.22}$$

then by varying the action (2.2) with respect to $\gamma_{\mu\nu}^{\text{CFT}}$ one can obtain a form of the boundary stress tensor [41]

$$T_{\text{CFT}}^{\mu\nu} \equiv \frac{2}{\sqrt{|\gamma_{CFT}|}}\frac{\delta S}{\delta\gamma_{\mu\nu}^{CFT}} = \frac{1}{8\pi G_N}\frac{r_c^3}{l_{\text{AdS}}^3}\gamma^{\mu\nu}\Big(r^\lambda\nabla_\lambda\Phi - \frac{\Phi}{l_{\text{AdS}}}\Big)|_{\partial M} \tag{2.23}$$

where $r_\lambda = \frac{l_{\text{AdS}}}{\sqrt{r^2-r_s^2}}\partial_\lambda r$ is the outward pointing (spacelike) unit normal form on the boundary and gives the units of (length)$^{-1}$ to the extrinsic curvature. The only nonzero component is r^r, which at the boundary is

$$r^r|_{\partial M} = \frac{r_c}{l_{\text{AdS}}}\sqrt{1-\Big(\frac{r_s}{r_c}\Big)^2} \approx \frac{r_c}{l_{\text{AdS}}}\Big(1-\frac{1}{2}\Big(\frac{r_s}{r_c}\Big)^2\Big) \tag{2.24}$$

as $r_c \to \infty$. The factors of l_{AdS} then cancel in the expression for the Hamiltonian on either boundary given by

$$H = T_{\text{CFT}}^{tt} = \frac{\Phi_h^2}{16\pi G_N \phi_b} \tag{2.25}$$

So the full Hamiltonian is the sum of the left and right Hamiltonians,

$$H = \frac{\Phi_h^2}{8\pi G_N \phi_b}. \tag{2.26}$$

The phase space can be written in terms of conjugate variables (E, δ) or (L, P), where L is the length variable and δ is the boundary difference time $\delta = (t_L + t_R)/2$. We now compute this renormalized geodesic length defined by

$$L = L_{bare} - L_c \tag{2.27}$$

where

$$L_{bare} = \int_{-x_c}^{x_c} \frac{dx}{\sqrt{1+(x/l_{\rm AdS})^2}}\,, \qquad L_c = 2l_{\rm AdS}\ln\left(2\frac{\phi_b r_c}{l_{\rm AdS}^2}\right). \tag{2.28}$$

We find x_c in terms of r_c by equating the Schwarzschild and global dilaton solutions at the boundary,

$$\frac{\phi_b r_c}{l_{\rm AdS}^2} = \Phi_h\sqrt{1+(x_c/l_{\rm AdS})^2}\cos(\tau/l_{\rm AdS}). \tag{2.29}$$

By setting $t_L = t_R \equiv t$, we can express $t = \delta$. Then using the relation between global and Schwarzschild times (2.16), we arrive at

$$x_c = l_{\rm AdS}\sqrt{(r_c/r_s)^2\cosh^2(\delta r_s/l_{\rm AdS}^2) - 1} \tag{2.30}$$

The integral in (2.28) evaluates to $L_{bare} = l_{\rm AdS}\ln\left(\frac{1+k}{1-k}\right)$ with

$$k \equiv \frac{x_c/l_{\rm AdS}}{\sqrt{1+(x_c/l_{\rm AdS})^2}} = \sqrt{1-\frac{1}{(r_c/r_s)^2\cosh^2(\delta r_s/l_{\rm AdS}^2)}} \approx 1 - \frac{1}{2(r_c/r_s)^2\cosh^2(\delta r_s/l_{\rm AdS}^2)} \tag{2.31}$$

in the limit $r_c \to \infty$. Therefore, $L_{bare} = l_{\rm AdS}\ln\big(4(r_c/r_s)^2\cosh^2(\delta r_s/l_{\rm AdS}^2)\big)$. Substituting the Schwarzschild radius from (2.10) into L_{bare}, we obtain for the full renormalized length (2.27)

$$L(\Phi_h) = 2l_{\rm AdS}\ln\left(\cosh\left(\frac{\delta\Phi_h}{\phi_b}\right)/\Phi_h\right), \tag{2.32}$$

which upon substituting $\Phi_h = \sqrt{8\pi G_N\phi_b E}$ from equation (2.26) gives the result in (2.21):

$$L(E) = 2l_{\rm AdS}\ln\left(\frac{\cosh\left(\sqrt{\frac{8\pi G_N E}{\phi_b}}\delta\right)}{\sqrt{8\pi G_N\phi_b E}}\right). \tag{2.33}$$

This is the Harlow-Jafferis semi-classical length [41]. Note that the variables E and Φ_h provide two representations of the geodesic length L, and therefore also wavefunctions $\psi(L)$. After defining the conjugate momentum through the Poisson bracket relation

$$\{L,P\}_{PB} = \frac{\partial L}{\partial\delta}\frac{\partial P}{\partial E} + \frac{\partial L}{\partial E}\frac{\partial P}{\partial\delta} \stackrel{!}{=} 1 \tag{2.34}$$

we can re-define the Hamiltonian in terms of $H(L,P)$ as

$$\begin{aligned} H &= \frac{8\pi G_N l_{\rm AdS}^2}{\phi_b}P^2 + \frac{1}{8\pi G_N\phi_b}e^{-L/l_{\rm AdS}} \\ &= \frac{P^2}{2m_{\rm eff}} + \frac{2l_{\rm AdS}^2}{\phi_b^2}m_{\rm eff}\,e^{-L/l_{\rm AdS}} \end{aligned} \tag{2.35}$$

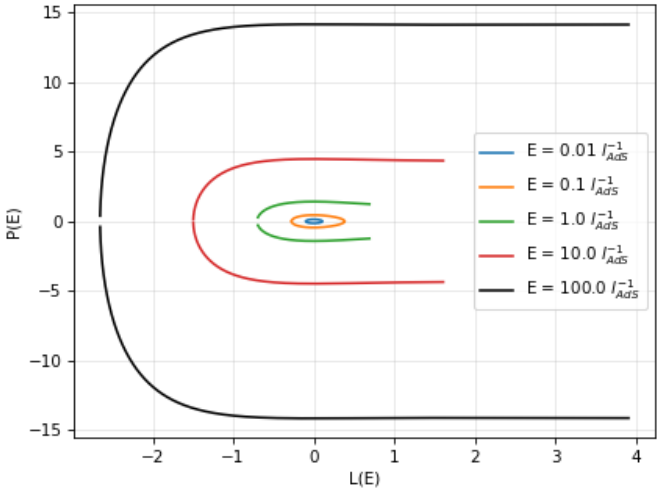

Figure 2.1: Phase space of JT gravity Hamiltonian

with the effective mass being

$$m_{\text{eff}} = \frac{\phi_b}{16\pi G_N l_{\text{AdS}}^2} \tag{2.36}$$

Evidently, in terms of this spacetime length L, JT becomes analogous to an exponentially decaying scattering potential as showin in figure 2.1.

We now want to consider measuring this renormalized geodesic distance L. For a given bulk state Ψ, the two basic measurement statistical quantities to calculate are the expectation value and variance,

$$\langle L \rangle_\Psi = \int_{-\infty}^{\infty} dL L |\psi(L)|^2 \,, \tag{2.37}$$

$$\left\langle L^2 \right\rangle_\Psi = \int_{-\infty}^{\infty} dL L^2 |\Psi(L)|^2 \,, \tag{2.38}$$

$$\left\langle (\Delta L)^2 \right\rangle_\Psi = \left\langle L^2 \right\rangle_\Psi - \langle L \rangle_\Psi^2 \,. \tag{2.39}$$

Below we compute the above with respect to the Hartle-Hawking state.

The Hartle-Hawking state Ψ_β has an associated inverse temperature β and is the analog of the thermofield double for JT. To derive an expression for $\Psi_\beta^{HH}(E)$ or $\Psi_\beta^{HH}(L)$ in either the E or L bases, Harlow and Jafferis find the saddle points of the Euclidean path integral. Here we just focus on the L basis calculation with the geometric constraints that the boundary region has length $\frac{r_c \beta}{2 l_{\text{AdS}}}$ and anchors a geodesic through the bulk of renormalized length L.

In the semi-classical limit $\phi_b/(\beta G_N) \gg 1$ the Hartle Hawking state becomes

$$\Psi_\beta(x)^{HH} = N \exp\left[\frac{2\pi\Phi_0 + \frac{8\phi_b}{\beta}\left(x^2 + \frac{2x}{\tan x}\right)}{16\pi G_N}\right], \tag{2.40}$$

where N is a normalization constant and $x \equiv \frac{r_s\beta}{4l^2_{\rm AdS}}$, where to get the second equality we used Eq. (2.9). The relationship between x and length L is given by

$$\frac{\sin x}{x} = 4\phi_b e^{L/(2l_{\rm AdS})}\beta^{-1}, \tag{2.41}$$

so that

$$L(x) = 2l_{\rm AdS}\ln\Big(\frac{\beta}{4\phi_b}\frac{\sin x}{x}\Big), \tag{2.42}$$

with $x \in [0, \pi]$.

The Hartle Hawking state (2.40) is approximately a Gaussian wave function peaked at $x_0 = \pi/2$ which corresponds to $L_{peak} := L(x_0) = 2l_{\rm AdS}\ln\left(\frac{\beta}{2\pi\phi_b}\right)$. In the semiclassical limit $\phi_b/(G_N\beta) \gg 1$ we can Taylor expand around $L = L_{peak}$. We obtain from (2.40) and (2.42)

$$\Psi^{HH}_\beta(L) \approx N e^{\frac{1}{8G_N}\left(\Phi_0 + \frac{\pi\phi_b}{\beta}\right)} e^{-\frac{\pi\phi_b}{32G_N\beta}\frac{(L-L_{peak})^2}{l^2_{\rm AdS}}}. \tag{2.43}$$

Computing the average length (2.37) and variance (2.39) in the HH state reduces to evaluating Gaussian integrals. The leading values in the semiclassical limit $\phi_b/(G_N\beta) \to \infty$ are

$$\langle L\rangle_\beta \approx 2l_{\rm AdS}\ln\Big(\frac{\beta}{2\pi\phi_b}\Big), \tag{2.44}$$

$$\big\langle(\Delta L)^2\big\rangle_\beta \approx l^2_{\rm AdS}\left(\frac{8G_N\beta}{\pi\phi_b}\right). \tag{2.45}$$

The fluctuations in the length are small compared to its average value as can be seen by combining (2.44) and (2.45) into the ratio

$$\frac{\Delta L}{L} = \frac{\sqrt{\frac{2G_N\beta}{\pi\phi_b}}}{\ln\left(\frac{\beta}{2\pi\phi_b}\right)} = \sqrt{16G_N}\frac{e^{L/(4l_{\rm AdS})}}{L/l_{\rm AdS}}, \tag{2.46}$$

which goes to zero in the semiclassical limit $(G_N\beta)/\phi_b \ll 1$. Note that we can rewrite the semiclassical limit as $L \ll -l_{\rm AdS}\log G_N$ which implies from (2.46) that $\Delta L/L \ll 1$. This makes sense since the length fluctuations must be small compared to the average length in the semi-classical limit.

Moreover, an interesting feature of the semi-classical limit is that it "squeezes" the length quadrature, in the language of quantum metrology. That is $\langle(\Delta L)^2\rangle_\beta \to 0$ as $G_N\beta/\phi_b \to 0$. In this regime, the JT Hamiltonian becomes entirely dominated by the potential term, which is consistent with the fact that $m_{\rm eff} \to \infty$ as $G_N \to 0$ as one can see from (2.36).

2.2 SYK Dual Length Operator

Taking Harlow and Jafferis' result for the length of a wormhole in JT, this leads us to ask: how can we measure it in the boundary CFT? For this, we need to identify its representation in the Sachdev Ye Kitaev (SYK) model, which resembles JT gravity in a low energy sector. First we provide a review of SYK and relevant scaling limits. Then we discuss representations for the length operator in SYK. Throughout we will either call the wormhole length L or ℓ, as will be clear by context.

Review of SYK and Scaling Limits

SYK is a chaotic many-body model consisting of N Majorana fermions ψ_i coupled by p-local random interactions J [76, 50]. The full SYK Hamiltonian is

$$\hat{H}_{SYK} = i^{p/2} \sum_{1 \le i_1 \le \cdots \le i_p \le N} J_{i_1 \ldots i_N} \psi_{i_1} \ldots \psi_{i_p} \,. \tag{2.47}$$

The couplings J are randomly sampled from a Gaussian distribution with zero mean and variance

$$\left\langle J^2_{i_1 \ldots i_p} \right\rangle = \frac{\mathcal{J}^2}{\lambda \binom{N}{p}} \tag{2.48}$$

where $\lambda = 2p^2/N$. The Majorana Fermion operators ψ_i satisfy

$$\{\psi_i, \psi_j\} = 2\delta_{ij} \,. \tag{2.49}$$

For more practical experimental implementations, often the more familiar $p = 4$ Hamiltonian is considered,

$$\hat{H}_{SYK} = \frac{1}{4 \cdot 4!} \sum_{i,j,k,l=1}^{N} J_{ijkl} \psi_i \psi_j \psi_k \psi_l \,. \tag{2.50}$$

An even further simplification can be made to this Hamiltonian known as the "complex SYK" model, in which the Fermions are modeled as spinless Dirac Fermions,

$$\hat{H}_c = \frac{1}{(2N)^{3/2}} \sum_{i_1, i_2, j_1, j_2 = 1}^{N} J_{i_1 i_2; j_1 j_2} c^\dagger_{i_1} c^\dagger_{i_2} c_{j_1} c_{j_2} - \mu \sum_i c^\dagger_i c_i \,. \tag{2.51}$$

with $\{c_i, c_i\} = 0, \{c_i, c_j\} = \delta_{ij}$, and μ a chemical potential [32].

Multiple pieces of evidence suggest that a regime of SYK might be dual to JT gravity because SYK i) saturates the chaos bound and ii) exhibits an effective Schwarzian action at low energies, which are two properties expected for JT gravity [70, 61].

We now review the double-scaled and triple-scaled limits of SYK, in which this correspondence with JT gravity becomes manifest and are therefore needed to define the wormhole length dual operator. An overview of these limits is shown in figure 2.2.

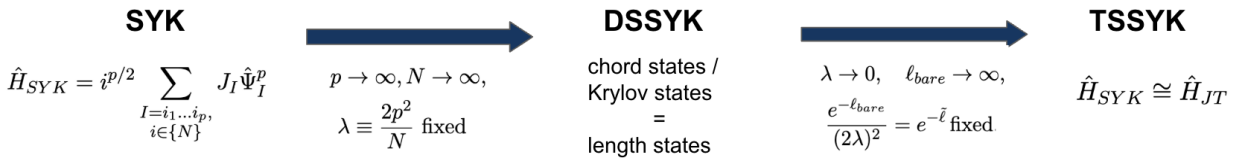

Figure 2.2: Overview of SYK Limits.

According to AdS/CFT, partition functions on the bulk spacetime and boundary CFT should match:

$$\mathrm{Tr}\big(e^{-\beta H_{CFT}}\big) = \mathrm{Tr}\big(e^{-\beta H_{AdS}}\big) \tag{2.52}$$

which can be decomposed into sums over moments of the Hamiltonian. Under this correspondence, there is a well-studied relation between triple-scaled SYK (TSSYK) and JT gravity. TSSYK is a limit of DSSYK, which we first review.

The *double-scaled limit* of SYK is where

$$p \to \infty, N \to \infty, \quad \lambda \equiv \frac{2p^2}{N} \text{ fixed}\,. \tag{2.53}$$

In this limit, the ensemble averaged moments of the Hamiltonian $\left\langle \mathrm{Tr}\left(\hat{H}_{SYK}^k\right)\right\rangle_J$ can be computed by using "chord diagrams" [55, 8]. Chord diagrams are combinatorial tools for calculating Wick contractions in moments of the Hamiltonian or higher order correlators. They are used as follows:

1. Given any correlation function $\mathrm{Tr}\big(O_1 e^{iHt} O_2 e^{-iHt}\ldots\big)$, decompose factors $e^{iHt} = \sum_k \frac{(iHt)^k}{k!}$ to be evaluated term by term.

2. Ensemble average and perform Wick contractions between couplings J in the Hamiltonians, and these are calculated using chord diagrams

When summing over chord diagrams, we count the number of intersecting chords between the various operators in the correlation function. Between two operators of sizes s_1 and s_2, [8] shows that one picks up contributions of $e^{-2s_1 s_2/N}$.

So for the case of moments of the Hamiltonian, which is an operator of size p, we pick up contributions of the form

$$e^{-2p^2/N} = e^{-\lambda} \equiv q \tag{2.54}$$

iterated over all possible chord diagrams. Therefore, the moments of the Hamiltonian are simply given by

$$m_k = \left\langle \mathrm{Tr}\big(H_{SYK}^k\big)\right\rangle_J = \sum_{\text{chord diagrams}} q^{\#\text{ H-H intersections}} \tag{2.55}$$

up to normalization factors.

For more complicated correlation functions involving insertions of operators M beyond the Hamiltonian [8],

$$\begin{aligned}&\left\langle \mathrm{tr}\left(\cdots H^{k_3} M_B H^{k_2} M_A H^{k_1}\right)\right\rangle_J \\ &= \sum_{\text{chord diagrams}} q^{\#H-H \text{ intersections}} \prod_A \left(e^{-2p_A p/N}\right)^{\#H-M_A \text{ intersections}} \prod_{A,B} \left(e^{-2p_A p_B/N}\right)^{\#M_A-M_B \text{ intersections}}\end{aligned} \tag{2.56}$$

These chord diagrams have an associated Hilbert space with an un-normalized "chord basis" $\{|n\rangle\}_{n=0}^{\infty}$, which represent the number of open chords. We can make a change of variables and define

$$\ell_{bare} \equiv l_{\mathrm{AdS}} \lambda n \tag{2.57}$$

so that the effective DSSYK Hamiltonian in the rescaled chord number basis becomes

$$\hat{T} = \frac{\mathcal{J}}{\sqrt{\lambda(1-q)}} \left(e^{i\lambda l_{\mathrm{AdS}} \hat{k}} \sqrt{1 - e^{-\hat{\ell}_{bare}/l_{\mathrm{AdS}}}} + \sqrt{1 - e^{-\hat{\ell}_{bare}/l_{\mathrm{AdS}}}} e^{-i\lambda l_{\mathrm{AdS}} \hat{k}}\right) \tag{2.58}$$

with $\hat{k} = \hat{p}/l_{\mathrm{AdS}}\lambda$ defined in terms of the conjugate momentum to $\hat{n}$ [55, 73, 4].

One can also make the chord basis orthonormal using a Gram-Schmidt type procedure. This amounts to carrying out a Lancoz algorithm which converts to the chord basis to a "Krylov basis."

Then in the *triple-scaled limit*, one further sends

$$\lambda \to 0, \ell_{bare} \to \infty, \quad \frac{e^{-\ell_{bare}}}{(2\lambda)^2} = e^{-\tilde{\ell}} \text{ fixed.} \tag{2.59}$$

This limit can be thought of as a choice of regularization scheme in the JT wormhole length picture. The third condition can be re-written as

$$\frac{\ell_{bare}}{l_{\mathrm{AdS}}} = \frac{\tilde{\ell}}{l_{\mathrm{AdS}}} - 2\log\left(\frac{1}{2\lambda}\right) \tag{2.60}$$

which is equivalent to the JT renormalization prescription when $\lambda = \frac{1}{2\sqrt{2}}\Phi|_{\partial M} = \frac{l_{\mathrm{AdS}}^2}{2\sqrt{2}\phi_b r_c}$ so $\lambda \to 0$ corresponds to $r_c \to \infty$, as expected in the semi-classical limit.

Hence, the triple-scaling limit effectively zooms into the low energy regime of SYK, resulting in the Hamiltonian

$$\hat{H} = E_0 + 2\lambda J\left(\frac{\hat{k}^2}{2} + 2e^{-\hat{\ell}/l_{\mathrm{AdS}}}\right) + \mathcal{O}(\lambda^2) \tag{2.61}$$

Note that the resulting triple-scaled $\hat{H}_{SYK}$ matches the form of $\hat{H}_{JT}$! Therefore, the triple scaled limit is often called the "quantum-JT" limit of SYK [57].

In addition to the double and triple scalings of SYK, another common scaling is called the *conformal limit*. Keeping in terms of the scaling parameter λ we defined above, the conformal limit can be formulated as [57]

$$\lambda \to 0, \quad \beta\mathcal{J} \to \infty, \quad C \equiv \frac{1}{\lambda\beta\mathcal{J}} = \frac{N}{2p^2\beta\mathcal{J}} \text{ fixed} \tag{2.62}$$

where βC provides the coefficient of the Schwarzian action. This coefficient C provides a metric for distinguishing between true quantum and semi-classical regimes of quantum JT gravity. For simplicity, let's set $\mathcal{J} = 1$ which we can do since it just sets the scale of the variance in the GUE and then the energy dependence will just be on β only. Then

$$C = \frac{1}{\beta\lambda} \ll 1 \longrightarrow \text{ quantum fluctuations of Scwharzian are large} \tag{2.63}$$

$$C = \frac{1}{\beta\lambda} \gg 1 \longrightarrow \text{ semi-classical regime} \tag{2.64}$$

So the quantum limit of JT is where we first take $\beta \to \infty$ and then $\lambda \to 0$ and the semi-classical regime is where we first take $\lambda \to 0$ and then $\beta \to \infty$. In the conformal limit, the SYK action becomes the Schwarzian,

$$S(\phi) = -\beta C \int du\{f(u), u\}. \tag{2.65}$$

Length as complexity or two-sided propagators

Now, we can discuss what the dual operator is in SYK for the length of a JT gravity wormhole. In general, we have found that there are two predominant ways of thinking formulating operators which probe wormhole length via: 1) complexity, and 2) two-point correlators across the sides subtending the length.

There have been many proposals which relate the volume of a wormhole in the bulk to the computational *complexity* of states in the boundary [13]. One manifestation of this connection between complexity and length is manifest from the double and triple scaling limits of SYK discussed in the previous section. As a reminder, in DSSYK we defined a length operator as a scaled version of the chord number operator,

$$\hat{\ell} = l_{\text{AdS}}\lambda\hat{n}. \tag{2.66}$$

Moreover, we showed that in TSSYK, this length operator takes the same form as the renormalized length operator $\tilde{\ell}$ as in JT gravity. However, the physical interpretation of chord number in terms of operators in SYK is unclear.

The authors in [4, 73] showed that there exists a more tangible formulation of this operator relation (2.66) in terms of Krylov complexity. Krylov complexity [74] is a measure of operator spreading in many-body systems exhibiting chaotic dynamics. Krylov complexity differs

from other measures of complexity by a choice of basis. The Krylov basis is chosen from the Baker-Campbell-Hausdorff expansion of the time evolution of an operator (or the moment expansion of the time evolution operator on a state), and is the optimal basis in the since that it provides an upper bound on for other complexity measures, analagous to quantum Fisher information versus classical Fisher information. More specifically, for Krylov complexity of a quantum state, we consider the expansion into moments

$$|\psi(t)\rangle = e^{-iHt}|0\rangle = \sum_{k=0}^{\infty} \frac{(-it)^k}{k!} H^k |0\rangle . \tag{2.67}$$

The Krylov basis is then obtained from a Gram-Schmidt orthonormalization procedure known as the Lanczos algorithm over the basis $\{H^k|0\rangle\}_{k=0}^{\infty}$. Thus intuitively, Krylov complexity probes the k at which is necessary to reconstruct a state $|\psi(t)\rangle$ from $|0\rangle$.

Notice that the basis $\{H^k|0\rangle\}_{k=0}^{\infty}$ is the chord basis discussed in the previous section. Therefore, the authors [4, 73] show that the Krylov basis is just an orthonormal version of the chord basis. They then define Krylov complexity C_K as the average chord number, $C_K = \langle \hat{n} \rangle$. This correspondence means that the length directly probes a form of operator spread complexity:

$$\left\langle \hat{\ell} \right\rangle = l_{\mathrm{AdS}} \lambda C_K, \tag{2.68}$$

with expectation value taken over the infinite-temperature thermofield double state in TSSYK. Given this correspondence, one can envision probing the length with experimental tools that diagnose Krylov complexity, such as OTOCs [74].

Alternatively, to derive a length operator directly in terms of SYK fermions, we can take a different approach using *two-sided propagators*. The length ℓ of the wormhole is the length between the left L and right R boundaries of JT gravity. In the thermofield double "ground state," this is simply the length across pure AdS_2. This is evident from the conventional holography ansatz

$$\left\langle \hat{\mathcal{O}}_L \hat{\mathcal{O}}_R \right\rangle = \int d\mathcal{P} e^{-\Delta L(\mathcal{P})} \tag{2.69}$$

where the propagator depends on the sum over geodesic paths $\mathcal{P}$ from L to R with lengths $L(\mathcal{P})$ [59, 5].

Thus, in order to probe the analog of this length in the boundary theory, we need a notion of left and right in an SYK system. The simplest way of doing this is two consider a system of two SYK Hamiltonians, H_{SYK}^L and H_{SYK}^R, which, using left as an example, can write as

$$\hat{H}_{SYK,L} = i^{p/2} \sum_{I}^{N} J_{I_p} \hat{\Psi}_{I_p}^L \tag{2.70}$$

using the shorthand $\Psi_{I_p} = \psi_{i_1} \dots \psi_{ip}$. Except in building up to the boundary representation from the bulk JT Hilbert space, how do we actually get this left-right operator distinction?

Section 3 of [55] and section 7 of [56] give an interesting answer via symmetry breaking: if we break the time translation symmetry between H_L and H_R, then this gives us a probe

of the length. One way of doing so is to insert a matter operator $\hat{\mathcal{O}}$ on the Euclidean disk. A general operator in one SYK with heaviness $\Delta = s/p$ can be written as

$$\hat{\mathcal{O}} = i^{s/2} \sum_I K_{I,s} \Psi_{I,s}, \tag{2.71}$$

$$\langle K_{i_1 \dots i_s} K_{j_1 \dots j_s} \rangle_J = \binom{N}{s}^{-1} \delta_{i_1 j_2} \dots \delta_{i_s j_s} \tag{2.72}$$

These operators are interpreted as "matter" fields in the bulk. This allows us to distinguish left and right chords on either side of $\hat{\mathcal{O}}$.

Concretely, as discussed in [55, 4],

$$e^{it\hat{H}_{SYK}} \hat{\mathcal{O}} e^{-it\hat{H}_{SYK}} |TFD\rangle \cong e^{it\hat{H}_L} e^{-it\hat{H}_R} |n_L = 0, n_R = 0\rangle = e^{-i(\hat{H}_R - \hat{H}_L)t} |0,0\rangle \tag{2.73}$$

where the $\cong$ means the two are equivalent under ensemble averaging either over the TFD or chords. Evidently, acting with $\hat{\mathcal{O}}$ amounts in a time evolution by $\hat{H}_R - \hat{H}_L$ which breaks the time translation symmetry.

We now use this fact to derive an expression such as (2.69) by considering the autocorrelation of $\hat{\mathcal{O}}$,

$$\mathcal{C}(t) = \left\langle \hat{\mathcal{O}} \hat{\mathcal{O}}(t) \right\rangle = \left\langle \mathrm{Tr}\left(\hat{\mathcal{O}} e^{i\hat{H}t} \hat{\mathcal{O}} e^{-i\hat{H}t} e^{-\beta \hat{H}} \right) \right\rangle_J \tag{2.74}$$

The correlator can be expanded into moments as

$$\mathcal{C}(t) = \left\langle \sum_{n=0}^{\infty} \frac{(it)^{2n}}{(2n)!} \mathrm{Tr}(\mathcal{O}[H,[H,\dots,[H,\mathcal{O}]\dots]]) \right\rangle_J \tag{2.75}$$

which involves terms

$$\begin{aligned}
\mathcal{C} \ni & \left\langle \mathrm{Tr}\left(\hat{\mathcal{O}} \hat{H}^{k_1} \hat{\mathcal{O}} \hat{H}^{k_2} \hat{H}^{k_3} \right) \right\rangle_J \\
&= \left\langle \mathrm{Tr}\left(\hat{\mathcal{O}} \hat{H}_L^{k_1} \hat{H}_R^{k_2} \right) \right\rangle_J \\
&= \sum_I i^{s/2} i^{p(k_1+k_2)/2} \frac{\left\langle K_{m_1 \dots m_s} (J^L_{i_1 \dots i_p})^{k_1} (J^R_{j_1 \dots j_p})^{k_2} \right\rangle_J}{\delta_{sp} \left(\mathcal{J}/\sqrt{\lambda \binom{N}{s}} \right)^{k_1+k_2}} \mathrm{Tr}\left(\hat{\Psi}_{I_s} (\hat{\Psi}^L_{I_p})^{k_1} (\hat{\Psi}^R_{I_p})^{k_2} \right) \\
&= \left[\frac{\mathcal{J}}{\sqrt{\lambda}} \binom{N}{s}^{-1/2} \right]^{k_1+k_2} \sum_I i^{s(k_1+k_2)/2} \mathrm{Tr}\left((\hat{\Psi}^L_{I_s})^{k_1} (\hat{\Psi}^R_{I_s})^{k_2} \right)
\end{aligned} \tag{2.76}$$

In the second line, we converted from an expectation value over the thermofield double state to chord states using (2.73). In the third line, we used a generalization of (2.48) and inferred that the action of a sole matter operator $\hat{\mathcal{O}}$ of size s on the TFD is to pick out a chord state of species s.

Note $k_1 + k_2 = 2n$ where $2n$ are the moments in the expansion of the correlator (2.75) [4]. If we consider up to the second moment $n = 1$, then

$$\mathcal{C} \ni \frac{\mathcal{J}^2}{\lambda}\binom{N}{s}^{-1} i^s \sum_I \mathrm{Tr}\Big(\hat{\Psi}^L_{I_s}\hat{\Psi}^R_{I_s}\Big) \tag{2.77}$$

Then using the chord diagram rule (2.56) which again is

$$\begin{aligned}&\big\langle \mathrm{tr}\left(\cdots H^{k_3} O_B H^{k_2} O_A H^{k_1}\right)\big\rangle_J \\ &= \sum_{\text{chord}} q^{\#H-H \text{ intersections}} \prod_A \Big(e^{-2p_A p/N}\Big)^{\#H-O_A \text{ intersections}} \prod_{A,B}\Big(e^{-2p_A p_B/N}\Big)^{\#O_A-O_B \text{ intersections}},\end{aligned} \tag{2.78}$$

and only considering $\mathcal{O} - H$ intersections[1], we get

$$\begin{aligned}\frac{\mathcal{J}^2}{\lambda}\binom{N}{s}^{-1} i^s \sum_I \mathrm{Tr}\Big(\hat{\Psi}^L_{I_s}\hat{\Psi}^R_{I_s}\Big) &= \sum_{\text{chords}} \prod_s \Big(e^{-2sp/N}\Big)^{\#\mathcal{O}-H \text{ intersections}} \\ &= e^{-2sp\tilde{n}/N} \\ &= e^{-\lambda\Delta\tilde{n}} \\ &= e^{-\Delta\ell/l_{\mathrm{AdS}}} \\ &= e^{-\Delta\langle\hat{\ell}\rangle/l_{\mathrm{AdS}}}\end{aligned} \tag{2.79}$$

where $\tilde{n} = n$ if there is no matter in the bulk.

Now we want to read off an operator relation from this equation involving traces on both sides of the equality. However, the ℓ on the right hand side is the expectation value $\left\langle\hat{\ell}\right\rangle = \lambda l_{\mathrm{AdS}}\langle\hat{n}\rangle = \lambda l_{\mathrm{AdS}} n$.

To make progress, we notice that

$$\Big\langle e^{-\hat{\ell}\Delta/l_{\mathrm{AdS}}}\Big\rangle = 1 - \frac{\Delta}{l_{\mathrm{AdS}}}\Big\langle\hat{\ell}\Big\rangle + \frac{1}{2}\Big(\frac{\Delta}{l_{\mathrm{AdS}}}\Big)^2\Big\langle\hat{\ell}^2\Big\rangle + \ldots \tag{2.80}$$

$$e^{-\langle\hat{\ell}\rangle\Delta/l_{\mathrm{AdS}}} = 1 - \frac{\Delta}{l_{\mathrm{AdS}}}\Big\langle\hat{\ell}\Big\rangle + \frac{1}{2}\Big(\frac{\Delta}{l_{\mathrm{AdS}}}\Big)^2\Big\langle\hat{\ell}\Big\rangle^2 + \ldots \tag{2.81}$$

so

$$\Big\langle e^{-\hat{\ell}\Delta/l_{\mathrm{AdS}}}\Big\rangle - e^{-\langle\hat{\ell}\rangle\Delta/l_{\mathrm{AdS}}} = \frac{1}{2}\Big(\frac{\Delta}{l_{\mathrm{AdS}}}\Big)^2 \mathrm{var}(\hat{\ell}) + O(\ell^3) \tag{2.82}$$

Therefore, to truly read off an operator relation from inside an expectation value we need to rearrange (2.79):

$$i^s\binom{N}{s}^{-1}\frac{\mathcal{J}^2}{\lambda}\sum_I \mathrm{Tr}\big(\Psi^s_{I,L}\Psi^s_{I,R}\big) = e^{-\Delta\langle\hat{\ell}\rangle/l_{\mathrm{AdS}}} = \Big\langle e^{-\Delta\hat{\ell}/l_{\mathrm{AdS}}} - \frac{1}{2}\Big(\frac{\Delta}{l_{\mathrm{AdS}}}\Big)^2\mathrm{var}(\hat{\ell})\Big\rangle \tag{2.83}$$

[1]This amounts to only considering free fields in the bulk

so we can now make an operator statement of the form

$$i^s \binom{N}{s}^{-1} \frac{\mathcal{J}^2}{\lambda} \sum_I \Psi^s_{I,L} \Psi^s_{I,R} = e^{-\Delta \hat{\ell}/l_{\text{AdS}}} - \frac{1}{2}\Big(\frac{\Delta}{l_{\text{AdS}}}\Big)^2 \text{var}(\hat{\ell}). \tag{2.84}$$

This is a modification of the relation proposed by Lin in [55], which accounts for the finite contribution of the variance of ℓ. Nontheless, it recovers the salient feature that Fermion bilinears of size s across two copies of SYK probe the exponential of the length of the wormhole.

To consider probing the length with the lightest possible fields in the bulk, we can choose $s = 1$ to get

$$\begin{aligned} \frac{i}{N}\frac{\mathcal{J}^2}{\lambda} \sum_{j=1}^N \psi^L_j \psi^R_j &= e^{-\Delta \hat{\ell}/l_{\text{AdS}}} - \frac{1}{2}\Big(\frac{1}{l_{\text{AdS}}\, p}\Big)^2 \text{var}(\hat{\ell}) \\ &= e^{-\Delta \hat{\ell}/l_{\text{AdS}}} - \frac{1}{l^2_{\text{AdS}} \lambda N} \text{var}(\hat{\ell}) \end{aligned} \tag{2.85}$$

In the triple scaled limit, this equation becomes

$$\frac{i}{N}\frac{\mathcal{J}^2}{\lambda} \sum_{j=1}^N \psi^L_j \psi^R_j = (2\lambda^2)^\Delta e^{-\Delta \hat{\tilde{\ell}}/l_{\text{AdS}}} - \frac{1}{l^2_{\text{AdS}} \lambda N} \text{var}(\hat{\tilde{\ell}}). \tag{2.86}$$

Thus, as more plainly seen by the case of $s = 1$, in the strict $N \to \infty$ limit we recover the form of the operator equation proposed by Lin [55].

Checks and analyses of the length operator

We can now check whether this operator equation recovers expected behavior before discussing how implement measurements of it on near-term quantum simulation platforms. As one check, we should see that at large N, the operator recovers the expected Schwinger-Dyson propagator for a two-sided SYK system. We now perform this calculation based off of [41, 77].

The large N solutions SYK can be written in terms of

$$G^{ij}(\tau) = \frac{1}{N}\sum_{a=1}^N G^{ij}_{aa}(\tau) = \frac{1}{N}\sum_{a=1}^N \left\langle \mathcal{T} \psi^i_a(\tau) \psi^j_a(0) \right\rangle, \tag{2.87}$$

$$\Sigma(\tau) \tag{2.88}$$

where G is the average two-point function and Σ is the self-energy (contains loop-level diagrams). In this notation, $i, j = L, R$ and a indexes fermion number. The two standard methods for calculating the G, Σ EOM are 1) solve the Schwinger-Dyson equation using melon diagrams (i.e. Feynman calculus for Majoranas) or 2) use the path integral.

We follow [41] and use the second method to compute the anneal-averaged Lorentzian path integral in Lorentzian time for the two systems.

$$\langle Z\rangle_J = \int DJD\psi \exp\left[-\frac{1}{2}\int dt \sum_{a,i}\psi_a^i\partial_t\psi_a^i + i\sum_I J_{I,p}\int dt\sum_i \Psi_{I,p}^i - \frac{1}{\mathcal{N}}\sum_I (J_{I,p})^2\right] \tag{2.89}$$

with $\mathcal{N} \equiv \langle J_{I,p}^2\rangle = \frac{\mathcal{J}^2}{\lambda\binom{N}{p}}$ as in (2.48). First compute the $\int DJ$ average just using Gaussian integration[2] to obtain

$$\langle Z\rangle_J = \sqrt{\mathcal{N}\pi}\int D\psi \exp\left[-\frac{1}{2}\int dt\sum_{a,i}\psi_a^i\partial t\psi_a^i - \frac{\mathcal{N}}{4}\sum_I\Big(\int dt\sum_i \Psi_{I,P}^i\Big)^2\right]. \tag{2.90}$$

Then we perform the Hubbard-Starcevich transformation and multiply by 1

$$1 = \int DG\delta(NG^{ij}(t,t') - \sum_a \psi_a^i(t)\psi_a^j(t')) \tag{2.91}$$

$$= \int DGD\Sigma \exp\left[-i\frac{N}{2}\int dt\int dt'\Sigma^{ij}\Big(G^{ij} - \frac{1}{N}\sum_a \psi_a^i(t)\psi_a^j(t')\Big)\right] \tag{2.92}$$

and also simplify the quadratic term in the partition function to be

$$\frac{\mathcal{N}}{4}\sum_I\Big(\int dt\sum_i \Psi_{I,P}^i\Big)^2 = \frac{\mathcal{N}}{4p!}\sum_I\int dt\int dt'\Big(G^{ij}(t,t')\Big)^p. \tag{2.93}$$

Now,

$$\langle Z\rangle_J \approx \sqrt{\mathcal{N}\pi}\int DGD\Sigma D\psi \exp\begin{bmatrix} -\frac{1}{2}\int dt\sum_{a,i}\psi_a^i\partial t\psi_a^i \\ -i\frac{N}{2}\int dt\int dt'\Sigma^{ij}\Big(G^{ij} - \frac{1}{N}\sum_a\psi_a^i(t)\psi_a^j(t')\Big) \\ -\frac{\mathcal{N}}{4p!}\sum_I\int dt\int dt'\Big(G^{ij}(t,t')\Big)^p \end{bmatrix} \tag{2.94}$$

Now that the exponential is bilinear in fermions, we can perform a Gaussian Berezin integral to get

$$\langle Z\rangle_J \approx \sqrt{N\pi}\int DGD\Sigma e^{-iNS_{eff}(G,\Sigma)} \tag{2.95}$$

with an effective action

$$S_{eff}(G,\Sigma) = i\log\big(\det\big(\delta_{ij}\partial_{t'} - i\Sigma^{ij}\big)\big) - \frac{N}{2}\sum_{i,j}\int dt\int dt'\Big(\Sigma^{ij}G^{ij} + \frac{i\mathcal{N}}{2N}(G^{ij})^p\Big) \tag{2.96}$$

[2] $\int dx e^{-ax^2+bx} = \sqrt{\pi/a}e^{b^2/4a}$

We now extremize the action to get the EOM,

$$0 = \delta S_{eff} = \frac{\partial S_{eff}}{\partial G}\delta G + \frac{\partial S_{eff}}{\partial \Sigma}\delta \Sigma. \tag{2.97}$$

Setting each partial derivative to 0 and using the identity

$$\nabla(\det A) = \det(A)A^{-1} \tag{2.98}$$

for any matrix A, we get the EOM

$$\Sigma^{ij} = i\mathcal{J}^2(G^{ij})^{p-1} \tag{2.99}$$

$$G = \frac{1}{\partial t - i\Sigma}. \tag{2.100}$$

Note this result is effectively already in the large N limit because the path integral (2.95) has saddle points for $N \to \infty$. Now we go to the conformal limit by also sending $\beta\mathcal{J} \to \infty$. Converting to Fourier space, the EOM become

$$\Sigma^{ij}(\omega) = i\mathcal{J}^2(G^{ij}(\omega))^{p-1} \tag{2.101}$$

$$G = \frac{1}{-i(\omega + \Sigma)}. \tag{2.102}$$

Low energy means $\omega \ll \mathcal{J}$ and since $\Sigma \propto \mathcal{J}^2$, we can neglect the $i\omega$ term in the second equation. Converting back to time space, we get

$$\Sigma^{ij}(t, t') = i\mathcal{J}^2(G^{ij}(t, t'))^{p-1} \tag{2.103}$$

$$\int dt'' G^{ij}(t, t'')\Sigma(t'', t) = i\delta(t - t') \tag{2.104}$$

The key insight is to now notice that in this limit, the master fields have a conformal symmetry that leaves the EOM invariant:

$$\Sigma^{ij}(t_1, t_2) \mapsto \Big(f_i'(t_1)f_j'(t_2)\Big)^{\Delta(p-1)}\Sigma_{ij}(f_i(t_1)f_j(t_2)) \tag{2.105}$$

$$G^{ij}(t_1, t_2) \mapsto \Big(f_i'(t_1)f_j'(t_2)\Big)^{\Delta}G_{ij}(f_i(t_1)f_j(t_2)). \tag{2.106}$$

This suggests we can use the ansatz for a Lorentzian correlator in conformal field theory as a solution,

$$G^{ij}(t_1, t_2) = \frac{b}{|i(t_1 - t_2)|^{2\Delta}}\text{sgn}(t_1 - t_2) \tag{2.107}$$

Now we want to consider specifically the left-right correlator $i = L, j = R$. If we assign

$$f_L(t_L) = -\frac{1}{\tanh\left(\frac{t_L}{2}\right)} \tag{2.108}$$

$$f_R(t_R) = \tanh\left(\frac{t_R}{2}\right) \tag{2.109}$$

then the conformal transformation in (2.106) yields after some trig algebra,

$$G^{LR}(t_L, t_R) = b\left[\frac{1}{2\cosh\left(\frac{t_L - t_R}{2}\right)}\right]^{2\Delta}(-1). \tag{2.110}$$

Hence, we recover the conformal propagator up to a minus sign. The negative sign comes from

$$\text{sgn}\Big(-\frac{1}{\tanh(t_L/2)} - \tanh(t_R/2)\Big) = -1 \tag{2.111}$$

for all $t_L = t_R > 0$. As such, we are inclined to adjust the length operator equation by an overall minus sign, or equivalently formulate it in terms of the two-sided propagator ordered as $\sum_{j=1}\left\langle \psi_j^R \psi_j^L \right\rangle = -\sum_{j=1}\left\langle \psi_j^L \psi_j^R \right\rangle$ given the anticommutation relations between Fermions

$$\{\psi_i^L, \psi_j^R\} = 0. \tag{2.112}$$

This negative redefinition of the operator is also consistent with numerical checks discussed in the next section.

We can now consider how to implement this operator in near-term digital and analog quantum simulators and derive predictions for measurement statistics that we can match with our bulk calculations.

2.3 Projective Measurement

The most simple form of measurement of the wormhole length one could perform is a projective measurement. This can be performed on digital quantum simulators, which implement discrete gates on an array of qubits. Specifically, we can exactly map Majorana fermions onto physical qubits via Jordan-Wigner transformations.

Digital qubit simulation

A system of N Majorana fermions can be encoded by $N/2$ conventional fermions classified by either even or odd site number [77],

$$\psi_{2j-1} = c_j + c_j^\dagger, \quad \psi_{2j} = c_j - c_j^\dagger \tag{2.113}$$

where $j \in \{1, \ldots, N/2\}$. Here we are using the following anticommutation relation conventions

$$\{\psi_i, \psi_j\} = 2\delta_{ij} \tag{2.114}$$

$$\{c_i, c_j\} = \{c_i^\dagger, c_j^\dagger\} = 0 \quad \{c_i, c_j^\dagger\} = \delta_{ij}. \tag{2.115}$$

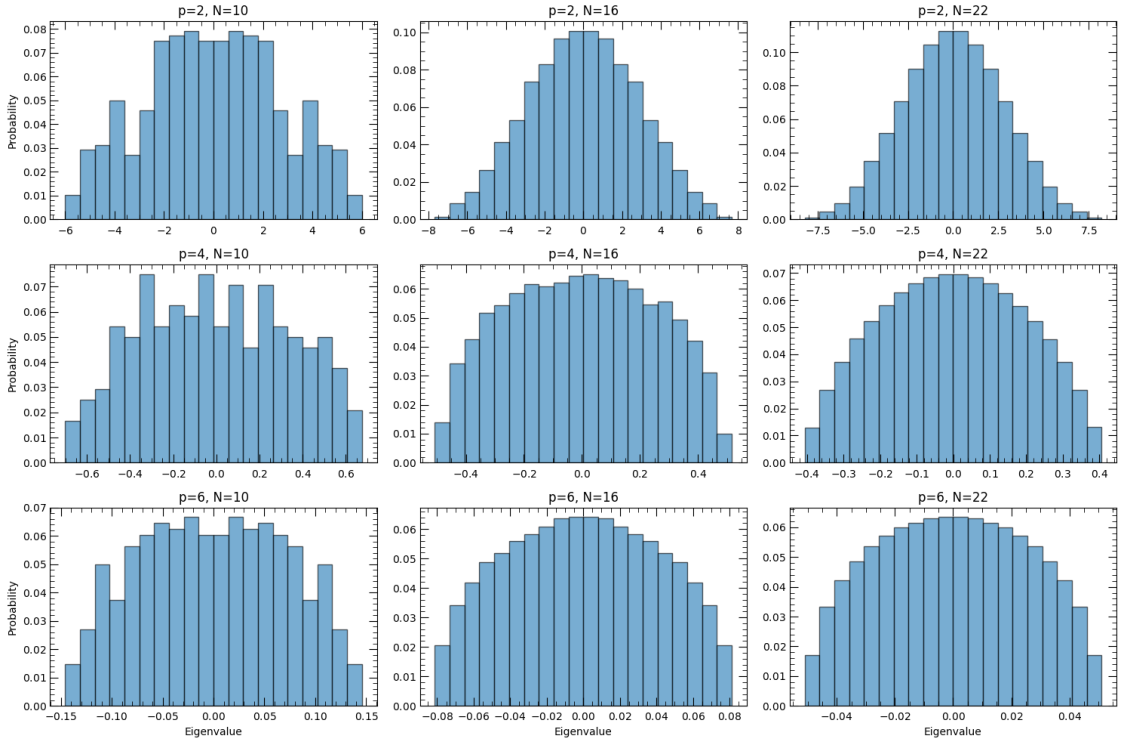

Figure 2.3: Numerical simulations of eigenspectrum for $\hat{H}_{SYK}$ with various p and N

The Jordan-Wigner transformation maps fermions c_i onto Pauli strings via

$$c_j = \Big(\prod_{k=1}^{j-1} \sigma_k^Z\Big)\sigma_j^-, \quad c_j^\dagger = \Big(\prod_{k=1}^{j-1} \sigma_k^Z\Big)\sigma_j^+ \tag{2.116}$$

with $\sigma_j^\pm = \frac{\sigma_j^X \pm \sigma_j^Y}{2}$. Using (2.113), we can express Majoranas in terms of Pauli strings through the mapping

$$\psi_{2j-1} = \left(\prod_{k=1}^{j-1} \sigma_j^Z\right)\sigma_j^X, \quad \psi_{2j} = \left(\prod_{k=1}^{j-1} \sigma_k^Z\right)\sigma_j^Y. \tag{2.117}$$

Then if we define the two-sided SYK operator

$$\hat{\mathcal{O}} \equiv \frac{i}{N}\sum_{j=1}^{N} \psi_j^L \psi_j^R = \frac{i}{N}\sum_{j=1}^{N}\left(\prod_{k=1}^{j-1} \sigma_k^Z\right)\sigma_j^{\alpha_j} \otimes \left(\prod_{k=1}^{j-1} \sigma_k^Z\right)\sigma_j^{\alpha_j}, \tag{2.118}$$

the length operator neglecting the finite $1/N$ contribution in (2.84) becomes

$$\hat{\ell} = -\frac{l_{\text{AdS}}}{\Delta}\log\Big(\hat{\mathcal{O}}\Big). \tag{2.119}$$

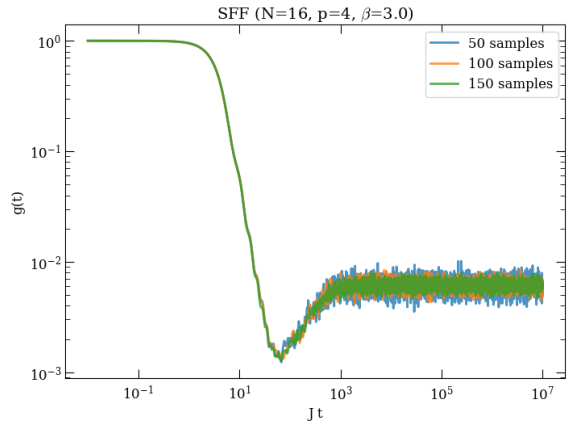

(a) Vary sample size

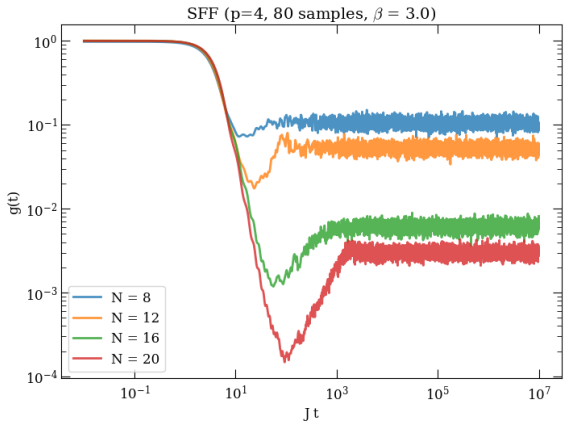

(b) Vary N

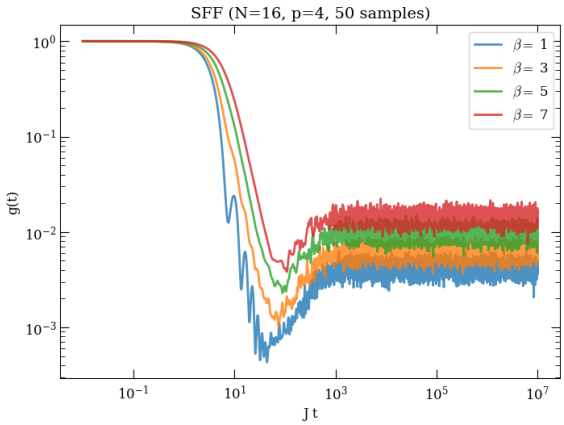

(c) Vary β

Figure 2.4: SYK spectral form factor simulations.

and for $s = 1$, $\hat{\ell} = -p\, l_{\text{AdS}} \log\left(\hat{\mathcal{O}}\right)$.

Now to simulate relevant measurement statistics such as $\left\langle \hat{\ell} \right\rangle$ and $\text{var}(\hat{\ell})$, we need a way to numerically simulate both the thermofield double state and the total SYK Hamiltonian $\hat{H} = \hat{H}_L + \hat{H}_R$.

For one copy of $\hat{H}_{L,R}$, we use the same Jordan Wigner transformation and randomly sample the couplings J from a GUE with the proper variance. Figure 2.3 shows the eigenspectrum for numerical simulations of an SYK Hamiltonian with the Jordan Wigner transformation (2.118) in Python. As expected, the smoothness of the spectrum increases as N increases. Moreover as p increases, we can observe the formation of the Wigner semi-circle law [77]

$$\rho(E) \propto \frac{1}{2\pi}\sqrt{4 - E^2} \tag{2.120}$$

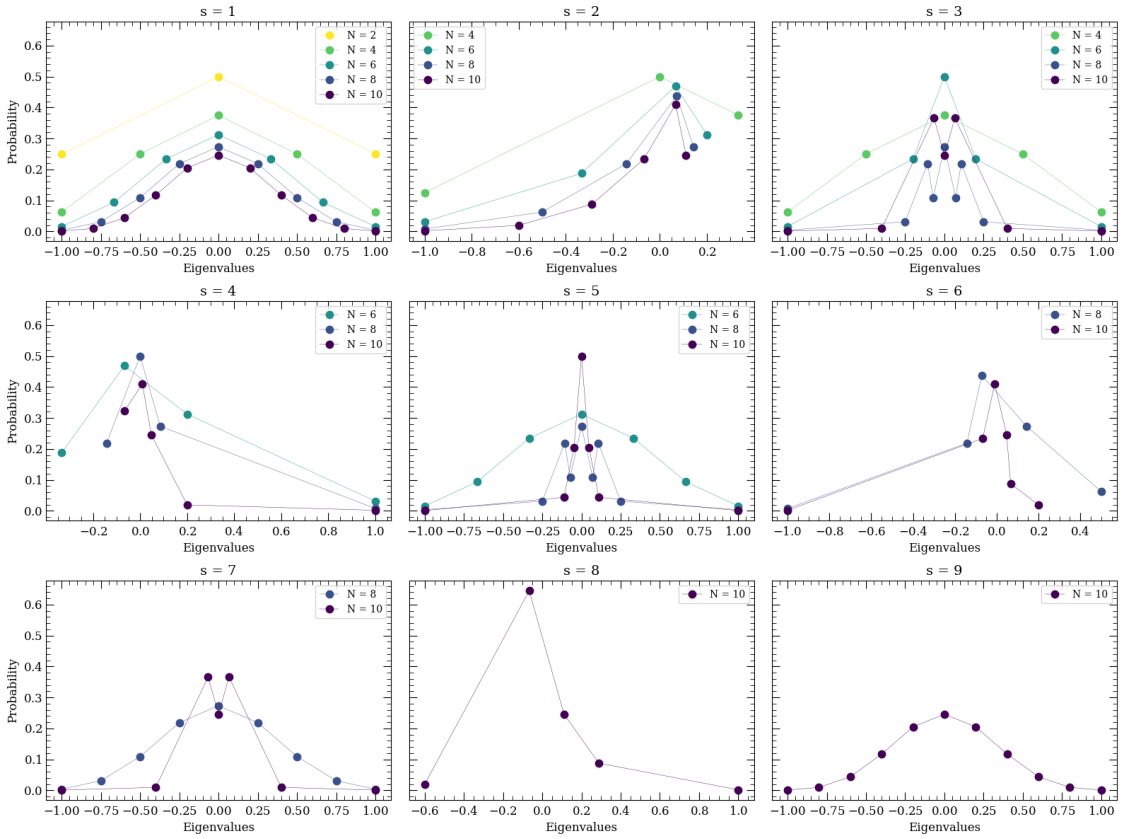

Figure 2.5: Eigenspectrum of the $\hat{\mathcal{O}}$ operator for various s and N.

which is expected from random matrix theory.

As a further check of our Hamiltonian, we simulated the Spectral Form Factor (SFF) [22]

$$g(t) = \frac{\langle Z(\beta,t)Z^*(\beta,t)\rangle}{\langle Z(\beta)\rangle_J^2} \tag{2.121}$$

where $Z(\beta,t) \equiv \mathrm{Tr}\left(e^{-\beta\hat{H}-i\hat{H}t}\right)$ is the analytically continued partition function. Figure 2.4 shows plots of SFF holding various combinations of N, β, and number of ensemble averages fixed. As shown, increasing the number of samples decreases the fluctuations. Increasing N drops the dip and ramp sections of the SFF. Increasing β decreases the ringing in the SFF, as all observed in [22].

Now to analyze the behavior of the operator $\hat{\mathcal{O}}$ involved in the length definition (2.119), we diagonalized the operator to find its eigenspectrum for various sizes s and number of fermions N as shown in figure 2.5. Odd values of s exhibit a symmetric distribution around 0. Even values of s skew the eigenspectrum either to the positive or negative side. In both

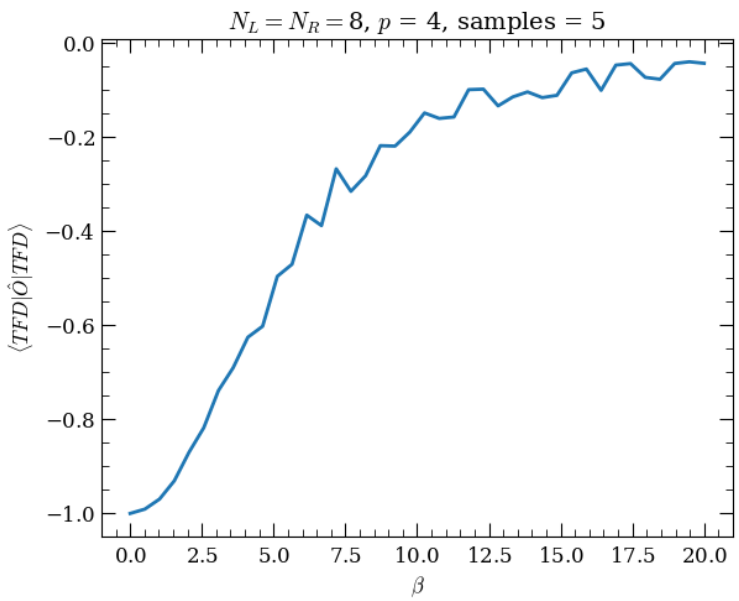

Figure 2.6: Simulations showing the negativity of $\left\langle \hat{O} \right\rangle_{TFD}$ across β.

cases, we can see that the eigenspectrum takes on negative values regardless of N, which is problematic for the argument of the logarithm.

One alternative discussed in [56] is that that for $N \to \infty$ and $\beta\mathcal{J} \to \infty$ limit, the spectrum of the propagator $\hat{O}$ in low energy states becomes uniformly positive. That is, we should see the spectrum shift towards positive eigenvalues under expectation values of the thermofield double state.

Constructing the thermofield double state

$$|TFD\rangle = \frac{1}{\sqrt{Z}} \sum_{n=1}^{N} e^{-\beta(E_L+E_R)/2} |n_L\rangle |n_R\rangle \tag{2.122}$$

experimentally is a non-trivial task [23]. As a close approximation, we follow Maldacena Qi [60] and use the thermofield double ansatz

$$|TFD\rangle = e^{-\beta/4(H_L+H_R)} |I\rangle \tag{2.123}$$

where $|I\rangle$ is the infinite temperature state defined by

$$\frac{1}{2}\left(\psi_j^L + i\psi_j^R\right) |I\rangle = 0 \quad \forall j. \tag{2.124}$$

In practice, $|I\rangle$ is a maximally entangled state between $\mathcal{H}_L \otimes \mathcal{H}_R$.

Performing the Jordan Wigner transformations discussed above onto both a left and right Hilbert space, our numerical simulations show that actually the expectation values

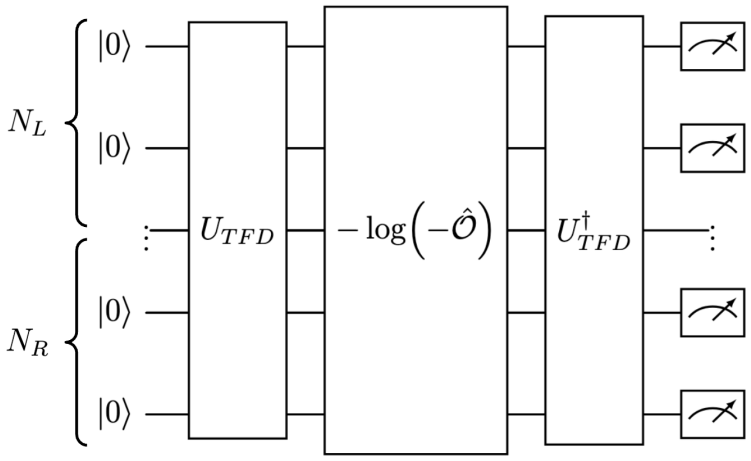

Figure 2.7: Digital quantum circuit implementation of $\left\langle \hat{\ell} \right\rangle_{TFD}$

$\left\langle \hat{O} \right\rangle_{TFD}$ are uniformly negative in β (see figure 2.6). Rather than becoming positive for lower temperatures, we instead see that at least for low N, the expectation value asymptotically approaches zero from -1 as $\beta \to \infty$. The fluctuations are due to finiteness in numerical sampling.

These numerics, along with the negativity of the analytical conformal result in (2.110), lead us to propose that the SYK definition for the length operator from [55] (with $s = 1$) should be modified to

$$e^{-\hat{\ell}\Delta/l_{\text{AdS}}} = -\frac{i}{N}\sum_{j=1}\psi_j^L\psi_j^R = \frac{i}{N}\sum_{j=1}\psi_j^R\psi_j^L. \tag{2.125}$$

so that we can now properly take the log.

Then using this definition, we can construct a quantum circuit that computes the expectation value $\langle TFD|\hat{\ell}|TFD\rangle$ as follows. The simplest way to get these measurement statistics is to perform a type of fidelity measurement, taking the inner product between the state $\hat{\ell}\,|TFD\rangle$ and $|TFD\rangle$. Equivalently, we can implement a circuit which transforms $\hat{\ell} = -\frac{l_{\text{AdS}}}{\Delta}\log\left(-\hat{\mathcal{O}}\right)$ into the thermofield double basis via conjugation of U_{TFD} where $U_{TFD}\,|0\rangle = |TFD\rangle$, as shown in figure 2.7.

To simulate the measurement statics from this revised operator definition in the thermofield double, we use a trick of converting the two-sided propagator into a one-sided one. Using the identities

$$\psi_j^L\,|I\rangle = -i\psi_j^R\,|I\rangle\,, \tag{2.126}$$

$$(H_L - H_R)\,|I\rangle = 0, \tag{2.127}$$

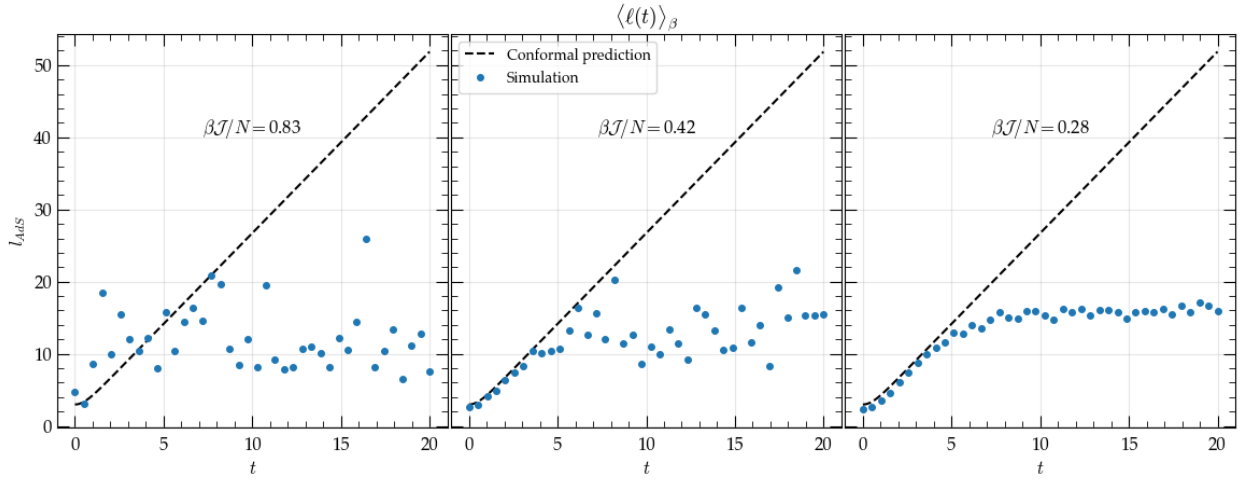

Figure 2.8: Numerical SYK simulations of wormhole length expectation value through time.

we can simplify

$$\begin{aligned} G_{LR}(t) &\equiv \frac{i}{N}\langle TFD|\sum_j \psi_j^L(t)\psi_j^R(t)|TFD\rangle \\ &= \frac{i}{N}\frac{1}{Z}\sum_j \langle I|e^{-\beta/4(H_L+H_R)}e^{i(H_L+H_R)t}\psi_j^L\psi_j^R e^{-i(H_L+H_R)t}e^{-\beta/4(H_L+H_R)}|I\rangle \\ &= \frac{i}{N}\frac{1}{Z}\sum_j \langle I|e^{(-\beta/2+2it)H_L}\psi_j^L\psi_j^R e^{-(\beta/2+2it)H_L}|I\rangle \\ &= -\frac{1}{N}\frac{1}{Z}\sum_j \langle I|e^{\beta H_L}\psi_j^L(\beta/2+2it)\psi_j^L(0)|I\rangle \\ &= -\frac{1}{N}\frac{1}{Z}\sum_j \mathrm{Tr}_L(\mathbb{1}_L e^{\beta H_L}\psi_j^L(\beta/2+2it)\psi_j^L(0)) \\ &= -\frac{1}{N}\sum_j \mathrm{Tr}_L(\rho_\beta\,\psi_j^L(\beta/2+2it)\psi_j^L(0)) \equiv G_{LL}(\beta/2+2it). \end{aligned} \tag{2.128}$$

Here we used also that $\{\psi_i^L, \psi_j^R\} = 0 \implies \left[H_L, \psi_j^R\right] = 0$, and that the trace over a maximally mixed state with operators only acting on the left side is equivalent to a trace over the identity operator only on the left side [71].

We are currently simulating measurement statistics of this wormhole length circuit using the simplified single-side correlator in (2.128), and preliminary results of these simulations are shown in figure 2.8. These plots show the time evolution of the wormhole length expectation value, for $N = 6, 12, 18$, $\beta = 5$, $p = 4$, and 3 ensemble averages. Evidently, in the conformal semi-classical limit as $\beta\mathcal{J}/N \to 0$ (the SYK analog of the JT semi-classical limit where

$G_N\beta/\phi_b \to 0$), the SYK numerics start to converge to the conformal Schwinger-Dyson prediction up until a plateau at approximately e^{S_0} [47]. Concretely, using the convention from [61], this dotted black line semi-classical prediction is

$$\frac{\langle \ell(t) \rangle}{l_{\text{AdS}}} = -4 \log \left(b \left[\frac{\pi}{\beta \cosh\left(\frac{2\pi t}{\beta}\right)} \right]^{1/2} \right), \quad b \approx 0.53 \tag{2.129}$$

and the blue dots are the simulation of

$$\frac{\langle \ell(t) \rangle}{l_{\text{AdS}}} = -4 \log(-G_{LL}(\beta/2 + 2it)). \tag{2.130}$$

We are scaling up these simulations to be implemented on the Lawrence Berkeley Lab NERSC supercomputer, so that we can achieve larger N, and also simulate the variance $\text{var}(\hat{\ell}) = \langle \hat{\ell}^2 \rangle - \langle \hat{\ell} \rangle^2$. Through these simulations, we will be able to compare finite-N results to our bulk measurement statics predictions in (2.44) and (2.45), and potentially provide a concrete experimental prediction for the N at which holographic geometric features begin to emerge in dual quantum mechanical systems.

2.4 Continuous Measurement

In addition to projective measurements, we can also consider continuously measuring the length operator in dual SYK systems. Such measurements are most feasibly implemented in analog simulation platforms, such as trapped ions or cold atom cavity-QED, in which quantum gates are implemented through continuous operations on an ensemble of molecules or atoms. Commonly, these interactions are often engineered using optical setups.

Accordingly, we can employ a technique known as "input-output theory" from quantum optics to calculate the variance in the measurement of the wormhole length. Input-output is analogous to an S-matrix formalism for quantum measurements, in which input light that scatters off of the system of interest picks up relevant phase information that is read out in the outgoing light [87]. In fact, by extremizing this variance calculated from linear response theory in input-output, we can derive an estimate of the wormhole length "standard quantum limit"—the minimal uncertainty allowed by Heisenberg uncertainty in measuring the length.

Toy measurement model

To motivate the procedure for analyzing the measurement theory of wormhole length in more realistic analog simulators, we first start with a toy model. Consider the renormalized JT gravity wormhole length coupled to a coherent drive of probe light as shown in figure 2.9. In this section we use the notation L for wormhole length. We model the incoming light and scattered light as a quantum mechanical bath, made up of harmonic oscillators.

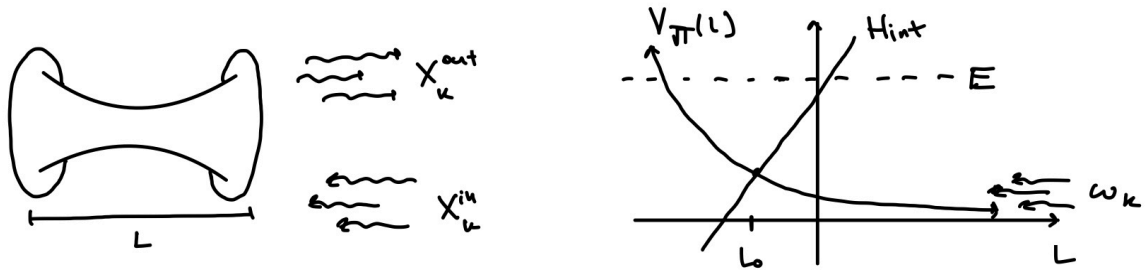

Figure 2.9: Schematic of toy model of continuous measurement of the wormhole length.

We can model the full system-bath-interaction Hamiltonian $\hat{H} = \hat{H}_{JT} + \hat{H}_b + \hat{H}_{int}$ as

$$\hat{H} = \frac{\hat{P}^2}{2m_{\text{eff}}} + \frac{2l_{\text{AdS}}^2}{\phi_b^2} m_{\text{eff}}\, e^{-\hat{L}/l_{\text{AdS}}} + \sum_k \omega_k b_k^\dagger b_k - i\sqrt{2}\sum_k g_k \hat{L}\hat{X}_k. \tag{2.131}$$

Here we posit a linear coupling g_k between the position $\hat{L}$ and the bath quadratures $\hat{X}_k = (\hat{b}_k + \hat{b}_k^\dagger)/\sqrt{2}$ in modes k. We have chosen a phase convention for $\hat{H}_{int}$ in which g_k is purely imaginary for cleanliness in subsequent calculations. The bath modes satisfy $\left[b_i, \hat{b}_j^\dagger\right] = \delta_{ij}$, and $[L, b_j] = 0$.

Here we posit a linear coupling g_k between the position $\hat{L}$ and the bath quadratures $\hat{X}_k = (\hat{b}_k + \hat{b}_k^\dagger)/\sqrt{2}$ in modes k. We have chosen a phase convention for $\hat{H}_{int}$ in which g_k is purely imaginary for cleanliness in subsequent calculations. The bath modes satisfy $\left[b_i, \hat{b}_j^\dagger\right] = \delta_{ij}$, and $[L, b_j] = 0$.

The Heisenberg equations of motion $\dot{\mathcal{O}} = i[H, \mathcal{O}]$ for the system and bath are:

$$\dot{\hat{L}} = \hat{P}/m_{\text{eff}} \tag{2.132}$$

$$\dot{\hat{P}} = \frac{2l_{\text{AdS}} m_{\text{eff}}}{\phi_b^2} e^{-\hat{L}/l_{\text{AdS}}} + \sqrt{2}\sum_k g_k \hat{X}_k \tag{2.133}$$

$$\dot{\hat{X}}_k = \omega_k \hat{Y}_k \tag{2.134}$$

$$\dot{\hat{Y}}_k = -\omega_k \hat{X}_k + i\sqrt{2} g_k \hat{L} \tag{2.135}$$

The goal is to express $\hat{L}(t), \hat{P}(t)$ in terms of input and output field modes. To do so, we need to solve for the time evolution of the bath quadrature $\hat{X}_k(t) = (\hat{b}_k(t) + \hat{b}_k^\dagger(t))/\sqrt{2}$. Starting with $\hat{b}^\dagger(t)$,

$$\dot{\hat{b}}_k^\dagger = i\omega_k \hat{b}_k^\dagger + \sqrt{2} g_k \hat{L} \tag{2.136}$$

or equivalently

$$\Big(\frac{\partial}{\partial t} - i\omega_k\Big)\hat{b}_k^\dagger = \sqrt{2}g_k\hat{L} \tag{2.137}$$

which is a standard first order inhomogeneous ODE in scattering theory. Two Greens functions which satisfy it are

$$G_{in}(t,t') = \Theta(t-t')e^{i\omega_k(t-t')}\,, \tag{2.138}$$

$$G_{out}(t,t') = -\Theta(t'-t)e^{i\omega_k(t-t')} \tag{2.139}$$

where

$$\Theta(t-t') = \begin{cases} 1, & t-t'>0 \\ 0, & t-t'<0 \end{cases}, \qquad \frac{\partial\Theta(\tau)}{\partial\tau} = \delta(\tau) \tag{2.140}$$

is the Heavyside step function. For the "in" modes, solving the ODE with G_{in} yields

$$\begin{aligned}\hat{b}_k^\dagger(t) &= \hat{b}_k^\dagger(t_0)e^{i\omega_k(t-t_0)} + \sqrt{2}\int_{t_0}^{t} dt' G_{in}(t,t')g_k\hat{L}(t') \\ &= \hat{b}_k^\dagger(t_0)e^{i\omega_k(t-t_0)} + \sqrt{2}\int_{-\infty}^{t} dt' e^{i\omega_k(t-t')}g_k\hat{L}(t').\end{aligned} \tag{2.141}$$

Similarly for $b_k(t)$ we get

$$\hat{b}_k(t) = \hat{b}_k(t_0)e^{-i\omega_k(t-t_0)} - \sqrt{2}\int_{-\infty}^{t} dt' e^{-i\omega_k(t-t')}g_k\hat{L}(t') \tag{2.142}$$

so $X_k(t) = (b_k(t) + \hat{b}_k^\dagger(t))/\sqrt{2}$ corresponding to the ingoing modes is

$$\hat{X}_k(t) = \frac{1}{\sqrt{2}}\Big(\hat{b}_k(t_0)e^{-i\omega_k(t-t_0)} + \hat{b}_k^\dagger(t_0)e^{i\omega_k(t-t_0)}\Big) + \int_{-\infty}^{t} dt'\Big(e^{i\omega_k(t-t')} - e^{-i\omega_k(t-t')}\Big)g_k\hat{L}(t'). \tag{2.143}$$

Inserting this expression into the momentum dynamics (2.133),

$$\begin{aligned}\dot{\hat{P}} = \frac{2l_{\rm AdS}m_{\rm eff}}{\phi_b^2}e^{-\hat{L}/l_{\rm AdS}} &- \sum_k g_k\Big(\hat{b}_k(t_0)e^{-i\omega_k(t-t_0)} + \hat{b}_k^\dagger(t_0)e^{i\omega_k(t-t_0)}\Big) \\ &+ \sqrt{2}\int_{-\infty}^{t} dt' \sum_k |g_k|^2\Big(e^{i(\omega_k+\omega_c)(t-t')} - e^{-i(\omega_k-\omega_c)(t-t')}\Big)e^{-i\omega_c(t-t')}\hat{L}(t').\end{aligned} \tag{2.144}$$

In the last term we have included some characteristic frequency ω_c of the system, which will be used momentarily to make the Markov approximation and the rotating wave approximation (RWA).

In standard quantum optics input-output theory, ω_c would be the fixed cavity resonant frequency. In JT, it is not immediately clear what this parameter should be. One natural

solution is to set ω_c to be the mechanical frequency when approximating V_{JT} as an oscillator around the equilibrium position L_0,

$$\omega_c = \omega_m = \frac{\sqrt{2}}{\phi_b} e^{-L_0/2l_{\rm AdS}} \,. \tag{2.145}$$

The Markov approximation is valid when

$$|\omega_k - \omega_c|(t - t') \gg 1. \tag{2.146}$$

This relationship can be satisfied when driving the system on resonance and considering late time measurements. As such, we assume that by measuring the wormhole length with a coherent drive and negligible detuning, $\Delta = \omega_c - \omega_d \approx 0$, we equilibrate the wormhole length around its harmonic oscillator equilibrium

$$L_0 = \langle L \rangle + \delta L \tag{2.147}$$

In this case, we should expect that any transients δL from radiation pressure will average out to a constant value over long measurement times so (2.146) holds.

We are still left with the counter-rotating term (the first term in the last line of (2.144)), which is taken care of with the RWA. The RWA is valid when

$$\Delta\omega = \omega_k - \omega_c \ll \omega_k + \omega_c \tag{2.148}$$

Therefore, we can take[3]

$$g_k = g \equiv \sqrt{\kappa} \tag{2.149}$$

to be constant over frequencies, which allows us to define

$$\hat{X}^{in}(t) \equiv \sum_k \frac{1}{\sqrt{2}} \Big(\hat{b}_k(t_0) e^{-i\omega_k(t-t_0)} + \hat{b}_k^\dagger(t_0) e^{i\omega_k(t-t_0)} \Big). \tag{2.150}$$

Then with the above approximations (i.e. Markov and RWA),

$$\begin{aligned} \dot{\hat{P}} \supset \sqrt{2} \int_{-\infty}^{t} dt' \sum_k |g_k|^2 \left(e^{i(\omega_k + \omega_c)(t-t')} - e^{-i(\omega_k - \omega_c)(t-t')} \right) e^{-i\omega_c(t-t')} \hat{L}(t') \\ = \sqrt{2}\kappa \int_{-\infty}^{t} dt' \left(e^{i\frac{\omega_k + \omega_c}{\omega_k - \omega_c}(t-t')} - 1 \right) \delta(t-t') e^{-i\omega_c(t-t')} \hat{L}(t') \\ = -\frac{\kappa}{\sqrt{2}} \hat{L}(t) \end{aligned} \tag{2.151}$$

since $\int_{-\infty}^{t} \delta(t - t')dt' = 1/2$ so (2.144) becomes

$$\dot{\hat{P}} = \frac{2 l_{\rm AdS} m_{\rm eff}}{\phi_b^2} e^{-\hat{L}/l_{\rm AdS}} - \sqrt{2\kappa} \hat{X}^{in}(t) - \frac{\kappa}{\sqrt{2}} \hat{L}(t) \,. \tag{2.152}$$

[3]Note that since g is purely imaginary, $\kappa = g^2 < 0$ in this convention.

Now we can repeat this process but for $\hat{X}^{out}(t)$, which are the field modes that we actually measure. Using the other Greens function $G_{out}(t,t')$ in (2.139), the time evolved "out" bath operators become

$$\hat{b}_k^\dagger(t) = \hat{b}_k^\dagger(t_1)e^{i\omega_k(t-t_1)} - \int_t^\infty dt' e^{i\omega_k(t-t')} g_k(\hat{L}(t') - L_0) \tag{2.153}$$

$$\hat{b}_k(t) = \hat{b}_k(t_1)e^{-i\omega_k(t-t_1)} + \int_t^\infty dt' e^{-i\omega_k(t-t')} g_k(\hat{L}(t') - L_0) \tag{2.154}$$

Note the integral terms have changed sign from the "in" counterparts (2.141)-(2.142) and the bounds are now defined the boundary conditions at future infinity $t_1 \to \infty$. Following the same approximations as above, we define the out modes as

$$X^{out}(t) \equiv \sum_k \frac{1}{\sqrt{2}}\Big(b_k(t_1)e^{-i\omega_k(t-t_1)} + \hat{b}_k^\dagger(t_1)e^{i\omega_k(t-t_1)}\Big) \tag{2.155}$$

and the momentum dynamics in terms of them becomes

$$\dot{P} = \frac{2l_{\text{AdS}}m_{\text{eff}}}{\phi_b^2}e^{-\hat{L}/l_{\text{AdS}}} - \sqrt{2\kappa}X^{out}(t) + \frac{\kappa}{\sqrt{2}}\hat{L}(t)\,. \tag{2.156}$$

Subtracting (2.156) from (2.160), we derive our *input-output relations*

$$\hat{X}^{out}(t) - \hat{X}^{in}(t) = \sqrt{\kappa}\hat{L}(t). \tag{2.157}$$

Now suppose that the input bath mode is a coherent laser with drive frequency ω_d such that

$$\hat{X}^{in}(t) = \left\langle \hat{X}^{in} \right\rangle + \hat{\xi}^{in}(t). \tag{2.158}$$

where $\left\langle \hat{X}^{in} \right\rangle$ is the classical contribution at ω_d and $\hat{\xi}^{in}(t)$ are the quantum fluctuations. We can configure $\left\langle \hat{X}^{in} \right\rangle$ such that the force of input bath on the particle with m_{eff} cancels out the force from the zeroth order constant term in V_{JT}, which occurs at the equilibrium position

$$L_0 = -l_{\text{AdS}} \ln\left(\sqrt{\frac{\kappa}{2}}\frac{\phi_b^2}{l_{\text{AdS}}m_{\text{eff}}}\left\langle \hat{X}^{in} \right\rangle\right) \tag{2.159}$$

Evidently, *the act of monitoring the wormhole by introducing a linear potential drive stabilizes its length.* This effect is shown in figure 2.9. Note if we set $\left\langle \hat{X}^{in} \right\rangle = 0$, then $L_0 = \infty$ which is the equilibrium that one would expect for the isolated wormhole when there is no bath coupled to it.

Expanding V_{JT} to first order around this equilibrium position, the momentum equation of motion becomes

$$\dot{\hat{P}} = -m_{\text{eff}}\omega_m^2(\hat{L}(t) - L_0) - \sqrt{2\kappa}\hat{\xi}^{in}(t) - \frac{\kappa}{\sqrt{2}}\hat{L}(t) \tag{2.160}$$

where

$$\omega_m = \frac{\sqrt{2}}{\phi_b} e^{-L_0/2l_{\rm AdS}} \tag{2.161}$$

is the mechanical frequency of $\hat{V}_{JT}$ when approximated as a harmonic oscillator.

The expected noise spectrum in measuring L is given by the *Power Spectral Density* (PSD), which is the Fourier transform of the autocorrelation function

$$S_{LL}(\omega) = \int dt e^{i\omega t} \left\langle \hat{L}(t)\hat{L}(0) \right\rangle \tag{2.162}$$

To derive it, we solve the equations of motion for $\hat{L}$ in frequency space and derive the relevant transfer functions.

The equations of motion in frequency space are

$$-i\omega L(\omega) = P(\omega)/m_{\rm eff} \tag{2.163}$$

$$-i\omega P(\omega) = F_0\,\delta(\omega) - \left(m_{\rm eff}\omega_m^2 + \frac{\kappa}{\sqrt{2}}\right)\hat{L}(\omega) - \sqrt{2\kappa}\hat{\xi}^{in}(\omega) \tag{2.164}$$

where we have labeled the constant term

$$F_0 = m_{\rm eff}\,\omega_m^2 L_0 \tag{2.165}$$

Solving (2.163) - (2.164) algebraically, we arrive at

$$L(\omega) = \chi_{LX}\Big(F_0\delta(\omega) - \sqrt{2\kappa}\hat{\xi}^{in}(\omega)\Big) \tag{2.166}$$

and we obtain for the transfer function

$$\chi_{LX} \equiv \frac{1}{m_{\rm eff}(\omega_m^2 - \omega^2) + \frac{\kappa}{2}}\,. \tag{2.167}$$

Repeating this process for the output EOM (2.156), we can also get L in terms of $\hat{\xi}^{out}(\omega)$,

$$L(\omega) = \chi_{LX}^*\Big(F_0\delta(\omega) - \sqrt{2\kappa}\hat{\xi}^{out}(\omega)\Big). \tag{2.168}$$

Now putting the pieces together, we want to find an expression for the noise power spectral density (PSD) of L, $S_{LL}(\omega)$, as a result of measuring the output modes $X^{out}(\omega)$. To do this, we first relate S_{LL} to S_{XX}^{out} using (2.168) and the Wiener-Khinchin theorem,

$$\begin{aligned}
2\pi\delta(\omega-\omega')S_{LL}(\omega) &= \left\langle L^\dagger(\omega)L(\omega')\right\rangle \\
&= 2\pi\delta(\omega-\omega')2\kappa|\chi_{LX}|^2 S_{XX}^{out}(\omega) \\
&\qquad + \underbrace{|\chi_{LX}|^2\left\langle F_0^2\delta(\omega)\delta(\omega') - F_0\delta(\omega)\sqrt{2\kappa}\hat{\xi}^{out}(\omega') - F_0\delta(\omega')\sqrt{2\kappa}\hat{\xi}^{out}(\omega)^\dagger\right\rangle}_{\text{(cross terms from constant force in expanding about } L_0)} \\
&= 2\pi\delta(\omega-\omega')2\kappa|\chi_{LX}|^2 S_{XX}^{out}(\omega) + |\chi_{LX}|^2\left\langle F_0^2\delta(\omega) - 2\sqrt{2\kappa}F_0\hat{\xi}^{out}(\omega)\right\rangle
\end{aligned} \tag{2.169}$$

where we have simplified in the last line using delta functions and the hermiticity of X.

We now further express S_{XX}^{out} in terms of S_{XX}^{in}. From (2.157) and (2.166),

$$\hat{\xi}^{out}(\omega) = \chi_{XX}\hat{\xi}^{in}(\omega) + \sqrt{\kappa}\chi_{LX}F_0\delta(\omega) \tag{2.170}$$

where

$$\chi_{XX} \equiv 1 - \sqrt{2}\kappa\chi_{LX} \tag{2.171}$$

so S_{XX}^{out} becomes

$$\begin{aligned} 2\pi\delta(\omega-\omega')S_{XX}^{out}(\omega) &= \left\langle \hat{\xi}^{out}(\omega)^\dagger \hat{\xi}^{out}(\omega') \right\rangle \\ &= 2\pi\delta(\omega-\omega')|\chi_{XX}|^2 S_{XX}^{in}(\omega) \\ &\quad + \left\langle \kappa|\chi_{LX}|^2F_0^2\delta(\omega) + \sqrt{\kappa}F_0\hat{\xi}^{in}(\omega)(\chi_{XX}^*\chi_{LX} + \chi_{XX}\chi_{LX}^*) \right\rangle \end{aligned} \tag{2.172}$$

after again applying the delta functions and Hermiticity.

Substituting (2.172) into (2.169) and expressing $\hat{\xi}^{out}(\omega)$ in terms of $\hat{\xi}^{in}(\omega)$ via (2.170), we get

$$2\pi\delta(\omega-\omega')S_{LL}(\omega) = 2\pi\delta(\omega-\omega')2\kappa|\chi_{XX}|^2|\chi_{LX}|^2S_{XX}^{in}(\omega) + \left\langle \chi_1\hat{\xi}^{in} \right\rangle + \langle\chi_2\rangle \tag{2.173}$$

with

$$\chi_1 = 2\sqrt{\kappa}|\chi_{LX}|^2F_0\Big(\kappa\delta(\omega)(\chi_{XX}^*\chi_{LX} + \chi_{XX}\chi_{LX}^*) - \sqrt{2}\chi_{XX}\Big) \tag{2.174}$$

$$\chi_2 = |\chi_{LX}|^2F_0^2\delta(\omega)\Big(1 + 2\kappa^2|\chi_{LX}|^2 - 2\sqrt{2}\kappa\chi_{LX}\delta(\omega)\Big) \tag{2.175}$$

Evidently, because of the constant F_0 term, the noise PSD $S_{LL}(\omega)$ depends on expectation values $\left\langle \hat{\xi}^{in} \right\rangle$ of the ingoing bath quantum fluctuations.

To obtain the SQL, we now "extremize" the PSD $S_{LL}(\omega)$. That is, we assume the quantum fluctuations at late measurement times average out, $\left\langle \hat{\xi}^{in} \right\rangle = 0$ and take $\hat{X}^{in}$ to be a coherent state so that $S_{XX}^{in} = 1/2$. We also choose the minimal decay rate

$$|\kappa^*| = \frac{e^{-2L_0/l_{\mathrm{AdS}}}L_0^2}{64G_N^2l_{\mathrm{AdS}}^4\pi^2\phi_b^2}. \tag{2.176}$$

which solves

$$\frac{\partial S_{LL}(\omega^* = \omega_m)}{\partial\kappa} = 0 \tag{2.177}$$

All together, this yields

$$S_{LL}(\omega_m) = \frac{e^{2L_0/l_{\mathrm{AdS}}}G_N^2l_{\mathrm{AdS}}^4\phi_b^2}{L_0^2}. \tag{2.178}$$

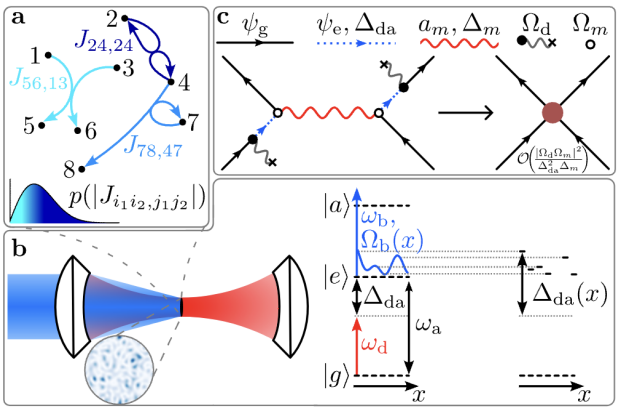

Figure 2.10: The SYK cold atom cavity model setup derived in [85]. The authors show how one can experimentally engineer the random couplings J spatialized speckled light pattern, with random detunings Δ_{da}.

Then we can approximate the SQL variance in L around a bandwidth $\Delta\omega = \omega_m$:

$$\begin{aligned}\Delta L^2_{SQL} &= \int_{-\infty}^{\infty} d\omega \frac{\sin^2(\omega t/2)}{\omega^2} S_{LL}(\omega) \approx \frac{t^2 S_{LL}(\omega_m)}{4}\omega_m \\ &\approx \frac{e^{\frac{5L_0}{2l_{\text{AdS}}}} G_N^2 l_{\text{AdS}}^4 \phi_b^3}{L_0^2}.\end{aligned} \tag{2.179}$$

where we have used $\sin(\omega t/2)/\omega^2 \approx t^2/4 - \mathcal{O}(\omega^2)$ and a measurement time of $t \approx 1/\omega_c$.

While this was a somewhat contrived toy model, it demonstrates how the techniques of input-output theory can be applied to determining the standard quantum limit of the length of the wormhole. Moreover, from this analysis we have gained some important pieces of intuition. Namely, that monitoring the wormhole with a linear drive that couples to its length can stabilize the otherwise exponentially decaying JT potential.

Analog cold atom cavity simulation

The authors of [85, 6] present a scheme for a cavity QED trapped cold atom setup which can be summarized as follows: two lasers are put into the cavity—the drive beam which traps the atoms, and the "light shift beam" which provides a speckled phase mask on the atoms, resulting in a spatially dependent AC stark shift. The resulting randomization of the atom-drive detuning $\Delta_{da} = \omega_d - \omega_a$ encodes the SYK couplings J. A diagram of this cavity setup is shown in figure 2.10.

In their setup, the model the drive lasers as classical and consider only the semi-classical Rabi oscillations which they induce in the fermion energy levels. For our purposes, we want to quantum mechanically model the measurement process. To do so, we need model the

incoming light as a bath of harmonic oscillators, dominated by a classical coherent drive component.

Two experimental configurations for this drive laser are possible: on-axis in line with the cavity, or off-axis from the cavity. In the former, the probe light will couple directly to the cavity modes, which then in turn couple to the atomic modes. In the latter, the probe light couples directly to the atomic modes. In what follows, we proceed with the on-axis drive setup for its greater simplicity in modeling the measurement process: the on-axis drive provides the bath which is used for homodyne detection for the wormhole length. In the off-axis drive case, we would to introduce a separate bath to perform this measurement.

Accordingly, the microscopic Hamtiltonian of the setup modified from the original presentation in [85] is:

$$\hat{H} = \hat{H}_{kt} + \hat{H}_c + \hat{H}_a + \hat{H}_d + \hat{H}_{ac} + \hat{H}_{cd}, \tag{2.180}$$

$$\hat{H}_{kt} = \sum_{s=e,g} \int d^2r \hat{\psi}^\dagger_{\rm s}(\boldsymbol{r}) \left(\frac{\boldsymbol{p}^2}{2m_{\rm at}} + V_{\rm t}(\boldsymbol{r}) \right) \hat{\psi}_{\rm s}(\boldsymbol{r}) \tag{2.181}$$

$$\hat{H}_c = \omega_c \hat{a}^\dagger \hat{a} \tag{2.182}$$

$$\hat{H}_a = \int d^2r \omega_{\rm a}(\boldsymbol{r}) \hat{\psi}^\dagger_{\rm e}(\boldsymbol{r}) \hat{\psi}_{\rm e}(\boldsymbol{r}) \tag{2.183}$$

$$\hat{H}_d = \sum_k \omega_k \hat{d}^\dagger_k \hat{d} \tag{2.184}$$

$$\hat{H}_{ac} = \frac{\Omega}{2} \int d^2r \left(g_c(\boldsymbol{r}) \hat{a} \psi^\dagger_{\rm e}(\boldsymbol{r}) \psi_{\rm g}(\boldsymbol{r}) + \text{ h.c.} \right) \tag{2.185}$$

$$\hat{H}_{cd} = i \sum_k g_k \left(\hat{a}^\dagger \hat{d}_k - \hat{d}^\dagger_k \hat{a} \right). \tag{2.186}$$

$\hat{H}_{kt}$ is the motional degree of freedom for the atomic center of mass, with ψ_g, ψ_e being the ground or excited field operators. The potential V_t is stated to be the harmonic trap potential. $\hat{H}_c$ is the cavity, $\hat{H}_a$ is the energy of the excited state of the atom with frequency ω_a, and $\hat{H}_d$ is the drive beam. $\hat{H}_{ac}$ and $\hat{H}_{cd}$ are the atom-cavity and cavity-drive interaction terms, with Ωf_c and g_k being the respective coupling strengths. We have assumed a generic damped driven cavity-drive interaction for $\hat{H}_{cd}$ with g_k real.

Suppose that the drive frequency of the laser is set to ω_d. We now go to a frame co-rotating with ω_d via the transformation

$$\hat{H} \to \hat{U}^\dagger \hat{H} \hat{U} - \hat{H} \tag{2.187}$$

with $\hat{U}$ generated by [87, 20]

$$\hat{H}_{RF} = \omega_d \int d^2r \hat{\psi}^\dagger_e \hat{\psi}_e + \omega_d \hat{a}^\dagger \hat{a} + \omega_d \sum_k \hat{d}^\dagger_k \hat{d}_k. \tag{2.188}$$

After computing the Baker-Campbell-Hausdorff commutators, the rotating frame Hamiltonian yields[4]

$$\hat{H} = \hat{H}_{kt} + \Delta_{cd}\hat{a}^\dagger\hat{a} - \int d^2r\Delta_{da}(\boldsymbol{r})\hat{\psi}_e^\dagger\hat{\psi}_e + \sum_{k\neq d}\Delta_{kd}\hat{d}_k^\dagger\hat{d}_k + \frac{\Omega}{2}\int d^2r g_c\hat{a}\hat{\psi}_e^\dagger\hat{\psi}_g + g_c^*\hat{\psi}_g^\dagger\hat{\psi}_e\hat{a}^\dagger + i\sum_k g_k\Big(\hat{a}^\dagger\hat{d}_k - \hat{d}_k^\dagger\hat{a}\Big) \tag{2.189}$$

with $\Delta_{kd} = \omega_k - \omega_d$, $\Delta_{cd} = \omega_c - \omega_d$ and $\Delta_{da}(\boldsymbol{r}) = \omega_d - \omega_a(\boldsymbol{r})$.

Before expanding about a coherent drive, we should first understand how the drive field induces cavity losses. The equations of motion of $\hat{a}$ and $\hat{d}_k$ are

$$\dot{\hat{a}} = -i\Delta_{cd}\hat{a} - i\frac{\Omega}{2}\int d^2r g_c^*\hat{\psi}_g^\dagger\hat{\psi}_e + \sum_k g_k\hat{d}_k \tag{2.190}$$

$$\dot{\hat{d}}_k = -i\omega_k\hat{d}_k - g_k\hat{a}\,. \tag{2.191}$$

We can solve the $\hat{d}_k$ equation using either incoming or outgoing Green's functions. For the incoming modes,

$$\hat{d}_k(t) = \hat{d}_k(t_0)e^{-i\omega_k(t-t_0)} - g_k\int_{-\infty}^{t} dt' e^{-i(\omega_c-\omega_k)(t-t')}e^{-i\omega_c(t-t')}\hat{a}(t'). \tag{2.192}$$

We now make the Markov approximation by assuming that $|\omega_c - \omega_k|(t-t') \ll 1$ such that $e^{-i\omega_c(t-t')} \to \delta(t-t')$. In the Markov approximation we can also treat the couplings as roughly constant over frequencies so we can define the damping rate as $g_k = g \equiv \sqrt{\kappa}$. Hence,[5]

$$\hat{d}_k(t) = \hat{d}_k(t_0)e^{-i\omega_k(t-t_0)} - \frac{\sqrt{\kappa}}{2}\hat{a}(t)\,. \tag{2.193}$$

Substituting $\hat{d}_k(t)$ back into (2.190), the cavity equations of motion become

$$\dot{\hat{a}}(t) = \Big(-i\Delta_{cd} + \frac{\kappa}{2}\Big)\hat{a}(t) + \sqrt{\kappa}\hat{d}_{in} - i\frac{\Omega}{2}\int d^2r g_c^*\hat{\psi}_g^\dagger\hat{\psi}_e \tag{2.194}$$

with $\hat{d}_{in} \equiv \sum_k \hat{d}_k(t_0)e^{-i\omega_k(t-t_0)}$.

Now we assume the drive is a coherent laser and expand the bath and cavity modes as a classical part plus quantum fluctuations

$$\hat{a} \to \alpha + \hat{a} \tag{2.195}$$

$$\hat{d}_{in} \to \varepsilon + \hat{d} \tag{2.196}$$

[4]The cavity and drive operators transform as $\hat{U}^\dagger\hat{a}\hat{U} = \hat{a}e^{-i\omega_d t}$ and $\hat{U}^\dagger\hat{d}_k\hat{U} = \hat{d}_k e^{-i\omega_d t}$ so the time dependence cancels in counter-rotating terms.

[5]$\int_{-\infty}^{t} dt\delta(t-t') = 1/2$

where $\alpha = \mathrm{Tr}(\rho\hat{a})$ and $\varepsilon = \mathrm{Tr}\Big(\rho\hat{d}_{in}\Big)$. This form arises from transforming the Hamiltonian with displacement operators $\hat{H} \to \hat{D}^\dagger(\alpha)\hat{D}^\dagger(\varepsilon)\hat{H}\hat{D}(\varepsilon)\hat{D}(\alpha)$ [12]. Taking the expectation value of (2.194) and assuming that $\Big\langle i\frac{\Omega}{2}\int d^2r g_c^*\hat{\psi}_g^\dagger\hat{\psi}_e\Big\rangle = 0$, we can solve for

$$\alpha(t) = \alpha(t_0)\exp\Big[(-i\Delta_{cd} + \frac{\kappa}{2})(t-t_0)\Big] - \sqrt{\kappa}\varepsilon/(-i\Delta_{cd} + \kappa/2). \tag{2.197}$$

Assuming $t_0 \to -\infty$, this constraint on α and ε becomes

$$\alpha = \frac{\sqrt{\kappa}\varepsilon}{i\Delta_{cd} - \kappa/2} \tag{2.198}$$

Using this relation and plugging the coherent drive expansions back into (2.189), the Hamiltonian becomes

$$\hat{H} = \hat{H}_{kt} + \Delta_{cd}\hat{a}^\dagger\hat{a} - \int d^2r\Delta_{da}(\boldsymbol{r})\hat{\psi}_e^\dagger\hat{\psi}_e + \int d^2r(\tilde{\Phi}\hat{\psi}_e^\dagger\hat{\psi}_g + \hat{\psi}_g^\dagger\hat{\psi}_e\tilde{\Phi}^\dagger) + i\sqrt{\kappa}\Big(\hat{a}^\dagger\hat{d} - \hat{d}^\dagger\hat{a}\Big) + \hat{H}_{\text{stuff}} \tag{2.199}$$

with

$$\tilde{\Phi}(\boldsymbol{r}) = \frac{\Omega}{2}g_c(\boldsymbol{r})\Big(\hat{a} + \frac{\sqrt{\kappa}\varepsilon}{i\Delta_{cd} - \kappa/2}\Big). \tag{2.200}$$

If we assume that $\sqrt{\kappa} \gg \Delta_{cd}$, then $\alpha \approx -2\varepsilon/\sqrt{\kappa}$ and $\hat{H}_{\text{stuff}}$ has the form

$$\hat{H}_{\text{stuff}} = \Delta_{cd}\Big(4\frac{|\varepsilon|^2}{\kappa} - \frac{2\varepsilon^*}{\sqrt{\kappa}}\hat{a} - \frac{2\varepsilon}{\sqrt{\kappa}}\hat{a}^\dagger\Big) + i\Big(2\varepsilon\hat{d}^\dagger - 2\varepsilon^*\hat{d} + \sqrt{\kappa}\varepsilon\hat{a}^\dagger - \sqrt{\kappa}\varepsilon^*\hat{a}\Big). \tag{2.201}$$

Since the incoming drive is a coherent laser at frequency ω_d, we have also assumed that any fluctuations Δ_{kd} are negligible.

From (2.199), we can see that the cavity modes couple to $\hat{\psi}_e^\dagger\hat{\psi}_g$. We can now follow the procedure in [85] by performing the following steps: 1) adiabatically eliminate the excited state, 2) perform a Schriefer-Wolf transformation.

1) We assume $|\Delta_{da}(\boldsymbol{r})|$ to be the dominant energy scale and adiabatically eliminate the excited state, so that

$$\hat{\psi}_e = \frac{\tilde{\Phi}\hat{\psi}_g}{\Delta_{da}}. \tag{2.202}$$

In this case, the Hamiltonian (2.199) simplifies to

$$\hat{H} = \hat{H}_{kt} + \Delta_{cd}\hat{a}^\dagger\hat{a} + \int d^2r\frac{\tilde{\Phi}^\dagger\tilde{\Phi}}{\Delta_{da}}\hat{\psi}_g^\dagger\hat{\psi}_g + i\sqrt{\kappa}\Big(\hat{a}^\dagger\hat{d} - \hat{d}^\dagger\hat{a}\Big) + \hat{H}_{\text{stuff}}. \tag{2.203}$$

2) Now we re-arrange the Hamiltonian as $\hat{H} = \hat{H}_0 + \hat{V}$ with all cavity-atom interactions relegated to $\hat{V}$:

$$\hat{H}_0 = \hat{H}_{kt} + i\sqrt{\kappa}\Big(\hat{a}^\dagger\hat{d} - \hat{d}^\dagger\hat{a}\Big) + \Delta_{cd}\hat{a}^\dagger\hat{a} + \int d^2r\frac{\kappa|\Omega g_c(\boldsymbol{r})\varepsilon|^2}{\Delta_{da}(\kappa^2 - 4\,\Delta_{cd}^2)}\hat{\psi}_g^\dagger\hat{\psi}_g + \hat{H}_{\text{stuff}} \tag{2.204}$$

$$\hat{V} = \int d^2r\frac{|\Omega g_c(\boldsymbol{r})|^2}{4\Delta_{da}}\hat{a}^\dagger\hat{a}\hat{\psi}_g^\dagger\hat{\psi}_g + \hat{a}^\dagger\Theta^\dagger + \Theta\hat{a}. \tag{2.205}$$

with

$$\Theta = \int d^2r \frac{\Omega g_c(\boldsymbol{r})\sqrt{\kappa}\varepsilon^*}{\Delta_{da}(-2i\Delta_{cd}-\kappa)}\hat{\psi}_g^\dagger\hat{\psi}_g \tag{2.206}$$

Then we perform a Schrieffer-Wolf transformation, which decouples the atom degrees of freedom from the cavity degrees of freedom. Specifically, the transformation is $e^{\hat{S}}\hat{H}e^{-\hat{S}} = \hat{H}_0 + (\hat{V} + [\hat{S}, \hat{H}_0]) + [\hat{S}, V] + \dots$ with $\hat{S}$ chosen such that $\hat{V} + [\hat{S}, \hat{H}_0] = 0$.

As shown in [85], this Schrieffer-Wolf transformation will separate the Hamiltonian into a one-body and two-body terms. Then after performing a change two the spinless Dirac fermions

$$\psi_g(\boldsymbol{r}) = \sum_{i_1} \phi_{i_1}(\boldsymbol{r}) c_{i_1}, \tag{2.207}$$

the Hamiltonian takes the general form

$$\hat{H}_{eff} = \underbrace{\sum_{i_1} \epsilon_{i_1} \hat{c}_{i_1}^\dagger \hat{c}_{i_1}}_{(\hat{H}_1)} + \underbrace{\sum_{i_1 i_2 i_3 i_4} J_{i_1 i_2 j_1 j_2} \hat{c}_{i_1}^\dagger \hat{c}_{i_2}^\dagger \hat{c}_{j_1} \hat{c}_{j_2}}_{(\hat{H}_2)} . \tag{2.208}$$

where the couplings J are functions of the spatially randomized detunings Δ_{da} and the two-body term $\hat{H}_2$ provides the effective SYK Hamiltonian. In [85], they tune the one-body strengths ϵ_{i_1} so as to make the first term $\hat{H}_1$ vanish.

However for our present purpose of measuring the length operator, a slightly different approach will be worthwhile. In particular, the perturbation $\hat{V}$ above contains a relevant term

$$\hat{V} \ni \int d^2r \frac{|\Omega g_c(\boldsymbol{r})|^2}{4\Delta_{da}} \hat{a}^\dagger \hat{a} \hat{\psi}_g^\dagger \hat{\psi}_g \tag{2.209}$$

If we arrange the cavity setup such that half of the atoms are labeled as L and half of the atoms are labeled as R, then this term above provides a potential measurement probe of the wormhole length operator. Namely, the cavity photon occupation number operator $\hat{N} = \hat{a}^\dagger \hat{a}$ couples to a version of the exponentiated length operator $\int d^2r \hat{\psi}_g^\dagger \hat{\psi}_g$ with coupling $\frac{|\Omega g_c(\boldsymbol{r})|^2}{4\Delta_{da}}$.

Alternatively, instead of adiabatically eliminating the excited state, we can keep the excited fermionic in order to achieve an effective left-right SYK copy distinction with the following ansatz

$$\hat{\psi}_e \to \hat{\psi}^L \tag{2.210}$$

$$\hat{\psi}_g \to \hat{\psi}^R \tag{2.211}$$

In this "zipped" ordering of left-right fermions, we would instead recover a coupling of the form $\int d^2r \frac{|\Omega g_c(\boldsymbol{r})|^2}{4\Delta_{da}} \hat{a}^\dagger \hat{a} \hat{\psi}_e^\dagger \hat{\psi}_g$, which also provides a measurement probe of the wormhole length via cavity photon occupation number. In upcoming work, we will explicitly perform this computation, and apply the input-output techniques from the previous section to compute the wormhole length standard quantum limit in this more realistic cavity QED model.

Chapter 3

Future Directions

Here we briefly sketch some possible extensions of this thesis work or ideas it generated for further investigations of quantum measurements in quantum gravity.

3.1 Bulk measurements

What dynamical or geometric phenomena in the bulk arise from measurements in the boundary theory? Various investigations into this question have been conducted, either considering how quantum measurements work for a bulk observer or what bulk dual properties might exist for boundary measurement-theoretic quantities [45, 52, 1].

We can begin to make progress on this question from the formalism of measuring bulk holographic observables in SYK such as wormhole length discussed in the previous sections. Recall that the length operator definition (up to a minus sign) takes the form

$$\frac{i}{N}\sum_{j=1}^{N}\psi_j^L\psi_j^R = e^{-\ell\Delta/l_{\mathrm{AdS}}}. \tag{3.1}$$

In other wormhole literature, Jafferis and Gao [30] discovered a mechanism by which a wormhole could become traversable via a double trace deformation that sends negative energy into the bulk. Maldacena and Qi extended [60] this work and showed that one could model a traversable wormhole by introducing a coupling between two SYK systems of the form

$$H = H_L + H_R + H_{int}, \quad H_{int} = i\mu\sum_j \psi_j^L\psi_j^R. \tag{3.2}$$

Note that given our operator definition for ℓ, we see that

$$H_{int} = e^{-\ell\Delta/l_{\mathrm{AdS}}} \tag{3.3}$$

when $\mu = 1/N$. This connection opens up the possibility of interpreting the interaction energy which makes the wormhole traversable as being a measurement of its length.

Moreover, it was found in [67, 79] that introducing matter insertions into the path integral can have the effect of stabilizing the length of a wormhole. These same matter insertions were what we used following [55] to break the time translation symmetry of the bulk Hilbert space of DSSYK and re-derive the form of the length operator above. Similarly [40, 42] showed that the process of making the wormhole traversable is analogous to the splitting a Wilson line of a pair of charges, which can probe the length between them. It was discussed in [79] that these matter insertions have the same conglomerate effect as adding the Maldacena Qi non-local interaction which makes the wormhole traversable—namely that the length stabilizes.

We had observed this length stabilization effect in a separate context of continuously measuring the length of a wormhole. Thus, by making these connections between matter insertions, traversability of wormholes, and length stabilization more rigorous in future work, we can perhaps contribute an interpretation that the act of measurement of wormhole length in the boundary introduces a process by which a wormhole becomes traversable in the bulk.

Moreover, we can intepret this question regarding the connection between bulk and boundary measurements in a more field-theoretic sense. If we actually wanted the bulk phenomena directly corresponding to a continuous boundary measurement using quantum optics, we would need to explicitly introduce gauge fields into the JT action. By introducing this perturbation to models of JT gravity with matter [49], we will study what dynamical gravitational features arise from the measurement process.

3.2 Further measurements of Hawking radiation

We discussed protocols to model measuring the purity of Hawking radiation. We can further extend this analysis through the language of quantum channels. As explained, making the boundary conditions of AdS_2 absorptive has the same effect as coupling a heat bath with Hilbert space $\mathcal{H}_E$ to the black hole system $\mathcal{H}_S$. We can consider treating the black hole and bath as an open quantum system, defined by the Hamiltonian

$$H = H_S + H_E + H_{int} \tag{3.4}$$

where the black hole and environment are coupled via an interaction H_{int}. The general time evolution of an open quantum system in the Kraus representation is given by

$$\rho(t) = \sum_a K_a \rho(0) K_a^\dagger \,. \tag{3.5}$$

Under the Markov/stationary approximation, this leads to the familiar Lindblad "master equation"

$$\dot{\rho}(t) = -i[H_S, \rho(t)] + \sum_{a\geq 1} L_a \rho(t) L_a^\dagger - \frac{1}{2}\{L_a^\dagger L_a, \rho(t)\} \tag{3.6}$$

with Lindblad operators L_a.

Previous work shows that both Markovian (time-local) or non-Markovian (time-nonlocal) baths can produce features resembling black hole physics. In [35] they analyzed weakly coupled Markovian baths with temperature $T = 0$ and calculate that the von Neumann entropy $S(t) = -\operatorname{Tr}(\rho(t)\log\rho(t))$ can exhibit Page curve-like dynamics. The papers [18, 80, 24] consider the SYK model of black holes coupled to non-Markovian baths and similarly observe an effective Page curve. These non-Markovian environments, moreover, provide richer system-bath entanglement structure as they are characterized by either by finite nonzero temperature or a frequency dependent spectral function. They also seem apt for modeling black hole evaporation: similar to the Hayden-Preskill decoding protocol, non-Markovian systems contain "memory" of past modes.

One simple non-Markovian model to study would be SYK linearly coupled to a bath of harmonic oscillators:

$$H_S = H_{SYK} = \frac{1}{4!}\sum_{i,j,k,l=1}^{N} J_{ijkl}\chi_i\chi_j\chi_k\chi_l \tag{3.7}$$

$$H_E = \sum_i \omega_i b_i^\dagger b_i \tag{3.8}$$

$$H_{int} = k\sum_i \chi_i^\dagger b_i + b_i^\dagger \chi_i \tag{3.9}$$

where $k = G_N C/(3\phi_b)$ is the coupling between the black hole and bath derived in JT from [25].

We could then consider calculating the (PSD) of this interaction,

$$S_{kk}(\nu) = \int_{-\infty}^{\infty}\frac{dt}{2\pi}e^{-i\nu t}\left\langle k(t)k(0)\right\rangle_{noise}, \tag{3.10}$$

which gives an observable prediction of the black hole noise power, and can be used to calculate the decoherence dynamics $D(t)$ in a dephasing channel of the form

$$\rho(t) = \begin{pmatrix}\rho_{00}(0) & e^{-D(t)}\rho_{01}(0)\\ e^{-D(t)}\rho_{10}^*(0) & \rho_{11}(0)\end{pmatrix}. \tag{3.11}$$

3.3 QFT in curved spacetime measurements

Considering quantum fluctuations to a classical GR background has been a lucrative semi-classical framework for analyzing quantum gravity. In this context, "Unruh DeWitt" detectors have been derived, which provide a particle-in-a-box model of a detector with response function to be excited to energy E given by [86]

$$P(E) = |\left\langle E|m(0)|0\right\rangle|^2\int_{\infty}^{\infty}d\tau\int_{-\infty}^{\infty}d\tau' e^{-iE(\tau-\tau')}\left\langle\psi|\phi(x(\tau))\phi(x(\tau'))|\psi\right\rangle. \tag{3.12}$$

We could consider placing such detectors near a black hole or in an accelerating frame and consider the Glauber coherence functions it could detect. Derived by Roy Glauber [36], these coherence functions $g^{(n)}$ quantify coherences of a field and physically corresponds to the joint probability of detecting n photons at spacetime locations $(\mathbf{r_1}, t_1), ..., (\mathbf{r_n}, t_n)$. For the electromagnetic field, they are given by

$$G^{(n)}(\rho; x_1 \dots x_n) = \mathrm{Tr}\Big(\rho \hat{E}^-(x_1) \dots \hat{E}^-(x_n) \hat{E}^+(x_n) \dots \hat{E}^+(x_1)\Big) \tag{3.13}$$

and the normalized coherence functions are

$$g^{(1)}(\rho; x_1, x_2) = \frac{G^{(1)}(x_1, x_2)}{\sqrt{G^{(1)}(x_1, x_1) G^{(1)}(x_2, x_2)}} \tag{3.14}$$

$$g^{(2)}(\rho; x_1, x_2) = \frac{G^{(2)}(x_1, x_2; x_2, x_1)}{G^{(1)}(x_1, x_1) G^{(1)}(x_2, x_2)} \tag{3.15}$$

$$\vdots \tag{3.16}$$

$$g^{(n)}(\rho, x_1 \dots x_n) = \frac{G^{(n)}(x_1, \dots, x_n; x_n, \dots, x_1)}{G^{(1)}(x_1, x_1) \dots G^{(1)}(x_n, x_n)}. \tag{3.17}$$

It is a fascinating result of quantum optics that for a thermal Gibbs partition function $g^{(2)} = 2$; For a pure state that exhibits sub-Poissonian statistics, $g^{(2)} < 2$. Thus exploring the measurement statistics from detectors in curved spacetimes using models such as Unruh-DeWitt detectors could provide another way of analyzing the purity of Hawking radiation or other relevant gravity observables.

Bibliography

[1] Chris Akers et al. *The black hole interior from non-isometric codes and complexity*. 2022. arXiv: 2207.06536 [hep-th]. URL: https://arxiv.org/abs/2207.06536.

[2] Ahmed Almheiri and Joseph Polchinski. "Models of AdS_2 backreaction and holography". In: *JHEP* 11 (2015), p. 014. DOI: 10.1007/JHEP11(2015)014. arXiv: 1402.6334 [hep-th].

[3] Ahmed Almheiri et al. "The entropy of bulk quantum fields and the entanglement wedge of an evaporating black hole". In: *JHEP* 12 (2019), p. 063. DOI: 10.1007/JHEP12(2019)063. arXiv: 1905.08762 [hep-th].

[4] Marco Ambrosini et al. *Operator K-complexity in DSSYK: Krylov complexity equals bulk length*. 2025. arXiv: 2412.15318 [hep-th]. URL: https://arxiv.org/abs/2412.15318.

[5] Vijay Balasubramanian and Simon F. Ross. "Holographic particle detection". In: *Physical Review D* 61.4 (Jan. 2000). ISSN: 1089-4918. DOI: 10.1103/physrevd.61.044007. URL: http://dx.doi.org/10.1103/PhysRevD.61.044007.

[6] Rahel Baumgartner et al. *Quantum simulation of the Sachdev-Ye-Kitaev model using time-dependent disorder in optical cavities*. 2024. arXiv: 2411.17802 [quant-ph]. URL: https://arxiv.org/abs/2411.17802.

[7] Ron Belyansky et al. "Minimal Model for Fast Scrambling". In: *Physical Review Letters* 125.13 (Sept. 2020). ISSN: 1079-7114. DOI: 10.1103/physrevlett.125.130601. URL: http://dx.doi.org/10.1103/PhysRevLett.125.130601.

[8] Micha Berkooz et al. "Towards a full solution of the large N double-scaled SYK model". In: *Journal of High Energy Physics* 2019.3 (Mar. 2019). ISSN: 1029-8479. DOI: 10.1007/jhep03(2019)079. URL: http://dx.doi.org/10.1007/JHEP03(2019)079.

[9] Bruno Bertini and Lorenzo Piroli. "Scrambling in random unitary circuits: Exact results". In: *Physical Review B* 102.6 (Aug. 2020). ISSN: 2469-9969. DOI: 10.1103/physrevb.102.064305. URL: http://dx.doi.org/10.1103/PhysRevB.102.064305.

[10] M. S. Blok et al. "Quantum Information Scrambling on a Superconducting Qutrit Processor". In: *Phys. Rev. X* 11 (2 Apr. 2021), p. 021010. DOI: 10.1103/PhysRevX.11.021010. URL: https://link.aps.org/doi/10.1103/PhysRevX.11.021010.

[11] Adam Bouland, Tudor Giurgica-Tiron, and John Wright. *The state hidden subgroup problem and an efficient algorithm for locating unentanglement*. 2024. arXiv: 2410.12706 [quant-ph]. URL: https://arxiv.org/abs/2410.12706.

[12] Warwick P. Bowen and Gerard J. Milburn. *Quantum Optomechanics*. Boca Raton, FL: CRC Press, 2016. ISBN: 978-1-4822-8015-8.

[13] Adam R. Brown et al. "Holographic Complexity Equals Bulk Action?" In: *Physical Review Letters* 116.19 (May 2016). ISSN: 1079-7114. DOI: 10.1103/physrevlett.116.191301. URL: http://dx.doi.org/10.1103/PhysRevLett.116.191301.

[14] Winton Brown and Omar Fawzi. *Scrambling speed of random quantum circuits*. 2013. arXiv: 1210.6644 [quant-ph]. URL: https://arxiv.org/abs/1210.6644.

[15] Daniel Carney. *Notes for PHYS 250: Quantum Theory of Measurement*. 2024. URL: https://quantum-measurement.lbl.gov/teaching/phys-250-quantum-theory-of-measurement.

[16] Daniel Carney, Philip C E Stamp, and Jacob M Taylor. "Tabletop experiments for quantum gravity: a user's manual". In: *Classical and Quantum Gravity* 36.3 (Jan. 2019), p. 034001. ISSN: 1361-6382. DOI: 10.1088/1361-6382/aaf9ca. URL: http://dx.doi.org/10.1088/1361-6382/aaf9ca.

[17] Sitan Chen et al. *Exponential separations between learning with and without quantum memory*. 2021. arXiv: 2111.05881 [quant-ph]. URL: https://arxiv.org/abs/2111.05881.

[18] Yu Chen. "Entropy linear response theory with non-Markovian bath". In: *Journal of High Energy Physics* 2021.4 (Apr. 2021). ISSN: 1029-8479. DOI: 10.1007/jhep04(2021)215. URL: http://dx.doi.org/10.1007/JHEP04(2021)215.

[19] Talal Ahmed Chowdhury et al. "Capturing the Page curve and entanglement dynamics of black holes in quantum computers". In: *Nuclear Physics B* 1019 (Oct. 2025), p. 117112. ISSN: 0550-3213. DOI: 10.1016/j.nuclphysb.2025.117112. URL: http://dx.doi.org/10.1016/j.nuclphysb.2025.117112.

[20] Aashish A. Clerk. *Optomechanics and Quantum Measurement*. Les Houches lecture notes. Lecture notes from the 2015 Les Houches School on Optomechanics. Montréal, Québec, Canada: Department of Physics, McGill University, 2015. URL: https://clerkgroup.uchicago.edu/PDFfiles/AC_OptomechLesHouchesV2.pdf.

[21] Jordan Cotler et al. "Chaos, complexity, and random matrices". In: *Journal of High Energy Physics* 2017.11 (Nov. 2017). ISSN: 1029-8479. DOI: 10.1007/jhep11(2017)048. URL: http://dx.doi.org/10.1007/JHEP11(2017)048.

[22] Jordan S. Cotler et al. "Black holes and random matrices". In: *Journal of High Energy Physics* 2017.5 (May 2017). ISSN: 1029-8479. DOI: 10.1007/jhep05(2017)118. URL: http://dx.doi.org/10.1007/JHEP05(2017)118.

[23] William Cottrell et al. "How to build the thermofield double state". In: *Journal of High Energy Physics* 2019.2 (Feb. 2019). ISSN: 1029-8479. DOI: 10.1007/jhep02(2019)058. URL: http://dx.doi.org/10.1007/JHEP02(2019)058.

[24] Pouria Dadras and Alexei Kitaev. "Perturbative calculations of entanglement entropy". In: *Journal of High Energy Physics* 2021.3 (Mar. 2021). ISSN: 1029-8479. DOI: 10.1007/jhep03(2021)198. URL: http://dx.doi.org/10.1007/JHEP03(2021)198.

[25] Waheed A. Dar, Prince A. Ganai, and Nirmalya Kajuri. *Hawking Radiation in Jackiw-Teitelboim Gravity*. 2025. arXiv: 2408.08985 [hep-th]. URL: https://arxiv.org/abs/2408.08985.

[26] Netta Engelhardt and Elliott Gesteau. *Further Evidence Against a Semiclassical Baby Universe in AdS/CFT*. 2025. arXiv: 2504.14586 [hep-th]. URL: https://arxiv.org/abs/2504.14586.

[27] Netta Engelhardt et al. *Spoofing Entanglement in Holography*. 2024. arXiv: 2407.14589 [hep-th]. URL: https://arxiv.org/abs/2407.14589.

[28] Julius Engelsöy, Thomas G. Mertens, and Herman Verlinde. "An investigation of AdS_2 backreaction and holography". In: *JHEP* 07 (2016), p. 139. DOI: 10.1007/JHEP07(2016)139. arXiv: 1606.03438 [hep-th].

[29] Ruihua Fan et al. "Out-of-time-order correlation for many-body localization". In: *Science Bulletin* 62.10 (May 2017), pp. 707–711. ISSN: 2095-9273. DOI: 10.1016/j.scib.2017.04.011. URL: http://dx.doi.org/10.1016/j.scib.2017.04.011.

[30] Ping Gao, Daniel Louis Jafferis, and Aron C. Wall. "Traversable wormholes via a double trace deformation". In: *Journal of High Energy Physics* 2017.12 (Dec. 2017). ISSN: 1029-8479. DOI: 10.1007/jhep12(2017)151. URL: http://dx.doi.org/10.1007/JHEP12(2017)151.

[31] Ignacio GarcÃÂa-Mata, Rodolfo Jalabert, and Diego Wisniacki. "Out-of-time-order correlations and quantum chaos". In: *Scholarpedia* 18.4 (2023), p. 55237. ISSN: 1941-6016. DOI: 10.4249/scholarpedia.55237. URL: http://dx.doi.org/10.4249/scholarpedia.55237.

[32] L. García-Álvarez et al. "Digital Quantum Simulation of Minimal AdS/CFT". In: *Physical Review Letters* 119.4 (July 2017). ISSN: 1079-7114. DOI: 10.1103/physrevlett.119.040501. URL: http://dx.doi.org/10.1103/PhysRevLett.119.040501.

[33] Martin Gärttner, Philipp Hauke, and Ana Maria Rey. "Relating Out-of-Time-Order Correlations to Entanglement via Multiple-Quantum Coherences". In: *Phys. Rev. Lett.* 120 (4 Jan. 2018), p. 040402. DOI: 10.1103/PhysRevLett.120.040402. URL: https://link.aps.org/doi/10.1103/PhysRevLett.120.040402.

[34] Steven B. Giddings. *Quantum gravity observables: observation, algebras, and mathematical structure*. 2025. arXiv: 2505.22708 [hep-th]. URL: https://arxiv.org/abs/2505.22708.

[35] Jonas Glatthard. *Thermodynamics of the Page curve in Markovian open quantum systems*. 2025. arXiv: 2501.09082 [quant-ph]. URL: https://arxiv.org/abs/2501.09082.

[36] Roy J. Glauber. "The Quantum Theory of Optical Coherence". In: *Phys. Rev.* 130 (6 June 1963), pp. 2529–2539. DOI: 10.1103/PhysRev.130.2529. URL: https://link.aps.org/doi/10.1103/PhysRev.130.2529.

[37] Noah Goss et al. "High-fidelity qutrit entangling gates for superconducting circuits". In: *Nature Communications* 13.1 (Dec. 2022). ISSN: 2041-1723. DOI: 10.1038/s41467-022-34851-z. URL: http://dx.doi.org/10.1038/s41467-022-34851-z.

[38] Andi Gu et al. *Simulating quantum chaos without chaos*. 2024. arXiv: 2410.18196 [quant-ph]. URL: https://arxiv.org/abs/2410.18196.

[39] Daniel Harlow. *TASI Lectures on the Emergence of the Bulk in AdS/CFT*. 2018. arXiv: 1802.01040 [hep-th]. URL: https://arxiv.org/abs/1802.01040.

[40] Daniel Harlow. "Wormholes, emergent gauge fields, and the weak gravity conjecture". In: *Journal of High Energy Physics* 2016.1 (Jan. 2016). ISSN: 1029-8479. DOI: 10.1007/jhep01(2016)122. URL: http://dx.doi.org/10.1007/JHEP01(2016)122.

[41] Daniel Harlow and Daniel Jafferis. "The Factorization Problem in Jackiw-Teitelboim Gravity". In: *ArXiv* (2019). arXiv: 1804.01081 [hep-th]. URL: https://arxiv.org/abs/1804.01081.

[42] Daniel Harlow and Jie-qiang Wu. "Algebra of diffeomorphism-invariant observables in Jackiw-Teitelboim gravity". In: *Journal of High Energy Physics* 2022.5 (May 2022). ISSN: 1029-8479. DOI: 10.1007/jhep05(2022)097. URL: http://dx.doi.org/10.1007/JHEP05(2022)097.

[43] S. W. Hawking. "Breakdown of predictability in gravitational collapse". In: *Phys. Rev. D* 14 (10 Nov. 1976), pp. 2460–2473. DOI: 10.1103/PhysRevD.14.2460. URL: https://link.aps.org/doi/10.1103/PhysRevD.14.2460.

[44] Patrick Hayden and John Preskill. "Black holes as mirrors: quantum information in random subsystems". In: *Journal of High Energy Physics* 2007.09 (Sept. 2007), pp. 120–120. ISSN: 1029-8479. DOI: 10.1088/1126-6708/2007/09/120. URL: http://dx.doi.org/10.1088/1126-6708/2007/09/120.

[45] Idse Heemskerk et al. "Bulk and transhorizon measurements in AdS/CFT". In: *Journal of High Energy Physics* 2012.10 (Oct. 2012). ISSN: 1029-8479. DOI: 10.1007/jhep10(2012)165. URL: http://dx.doi.org/10.1007/JHEP10(2012)165.

[46] Pavan Hosur et al. "Chaos in quantum channels". In: *Journal of High Energy Physics* 2016.2 (Feb. 2016). ISSN: 1029-8479. DOI: 10.1007/jhep02(2016)004. URL: http://dx.doi.org/10.1007/JHEP02(2016)004.

[47] Luca V. Iliesiu et al. *On the non-perturbative bulk Hilbert space of JT gravity*. 2024. arXiv: 2403.08696 [hep-th]. URL: https://arxiv.org/abs/2403.08696.

[48] R. Jackiw. "Lower Dimensional Gravity". In: *Nucl. Phys. B* 252 (1985). Ed. by R. Baier and H. Satz, pp. 343–356. DOI: 10.1016/0550-3213(85)90448-1.

[49] Daniel Louis Jafferis et al. *JT gravity with matter, generalized ETH, and Random Matrices*. 2023. arXiv: 2209.02131 [hep-th]. URL: https://arxiv.org/abs/2209.02131.

[50] Alexei Kitaev. *A Simple Model of Quantum Holography*. Online talk at KITP: Entanglement in Strongly-Correlated Quantum Matter. Video available at https://online.kitp.ucsb.edu/online/entangled15/kitaev/. Apr. 2015.

[51] Bryce Kobrin et al. *A Universal Protocol for Quantum-Enhanced Sensing via Information Scrambling*. 2024. arXiv: 2411.12794 [quant-ph]. URL: https://arxiv.org/abs/2411.12794.

[52] Nima Lashkari and Mark Van Raamsdonk. "Canonical energy is quantum Fisher information". In: *Journal of High Energy Physics* 2016.4 (Apr. 2016), pp. 1–26. ISSN: 1029-8479. DOI: 10.1007/jhep04(2016)153. URL: http://dx.doi.org/10.1007/JHEP04(2016)153.

[53] Nima Lashkari et al. "Towards the fast scrambling conjecture". In: *Journal of High Energy Physics* 2013.4 (Apr. 2013). ISSN: 1029-8479. DOI: 10.1007/jhep04(2013)022. URL: http://dx.doi.org/10.1007/JHEP04(2013)022.

[54] R. J. Lewis-Swan et al. "Unifying scrambling, thermalization and entanglement through measurement of fidelity out-of-time-order correlators in the Dicke model". In: *Nature Communications* 10.1 (Apr. 2019). ISSN: 2041-1723. DOI: 10.1038/s41467-019-09436-y. URL: http://dx.doi.org/10.1038/s41467-019-09436-y.

[55] Henry W. Lin. "The bulk Hilbert space of double scaled SYK". In: *Journal of High Energy Physics* 2022.11 (Nov. 2022). ISSN: 1029-8479. DOI: 10.1007/jhep11(2022)060. URL: http://dx.doi.org/10.1007/JHEP11(2022)060.

[56] Henry W. Lin, Juan Maldacena, and Ying Zhao. "Symmetries near the horizon". In: *Journal of High Energy Physics* 2019.8 (Aug. 2019). ISSN: 1029-8479. DOI: 10.1007/jhep08(2019)049. URL: http://dx.doi.org/10.1007/JHEP08(2019)049.

[57] Henry W. Lin and Douglas Stanford. "A symmetry algebra in double-scaled SYK". In: *SciPost Physics* 15.6 (Dec. 2023). ISSN: 2542-4653. DOI: 10.21468/scipostphys.15.6.234. URL: http://dx.doi.org/10.21468/SciPostPhys.15.6.234.

[58] Zi-Wen Liu et al. "Entanglement, quantum randomness, and complexity beyond scrambling". In: *Journal of High Energy Physics* 2018.7 (July 2018). ISSN: 1029-8479. DOI: 10.1007/jhep07(2018)041. URL: http://dx.doi.org/10.1007/JHEP07(2018)041.

[59] Jorma Louko, Donald Marolf, and Simon F. Ross. "Geodesic propagators and black hole holography". In: *Physical Review D* 62.4 (July 2000). ISSN: 1089-4918. DOI: 10.1103/physrevd.62.044041. URL: http://dx.doi.org/10.1103/PhysRevD.62.044041.

[60] Juan Maldacena and Xiao-Liang Qi. *Eternal traversable wormhole*. 2018. arXiv: 1804.00491 [hep-th]. URL: https://arxiv.org/abs/1804.00491.

[61] Juan Maldacena and Douglas Stanford. "Remarks on the Sachdev-Ye-Kitaev model". In: *Physical Review D* 94.10 (Nov. 2016). ISSN: 2470-0029. DOI: 10.1103/physrevd.94.106002. URL: http://dx.doi.org/10.1103/PhysRevD.94.106002.

[62] Antonio Anna Mele. "Introduction to Haar Measure Tools in Quantum Information: A Beginneramp;apos;s Tutorial". In: *Quantum* 8 (May 2024), p. 1340. ISSN: 2521-327X. DOI: 10.22331/q-2024-05-08-1340. URL: http://dx.doi.org/10.22331/q-2024-05-08-1340.

[63] Thomas G. Mertens and Gustavo J. Turiaci. "Solvable models of quantum black holes: a review on Jackiw–Teitelboim gravity". In: *Living Reviews in Relativity* 26.1 (July 2023). ISSN: 1433-8351. DOI: 10.1007/s41114-023-00046-1. URL: http://dx.doi.org/10.1007/s41114-023-00046-1.

[64] Xiao Mi et al. "Information scrambling in quantum circuits". In: *Science* 374.6574 (Dec. 2021), pp. 1479–1483. ISSN: 1095-9203. DOI: 10.1126/science.abg5029. URL: http://dx.doi.org/10.1126/science.abg5029.

[65] Xiao Mi et al. "Time-crystalline eigenstate order on a quantum processor". In: *Nature* 601.7894 (Nov. 2021), pp. 531–536. ISSN: 1476-4687. DOI: 10.1038/s41586-021-04257-w. URL: http://dx.doi.org/10.1038/s41586-021-04257-w.

[66] A. Morvan et al. "Qutrit Randomized Benchmarking". In: *Physical Review Letters* 126.21 (May 2021). ISSN: 1079-7114. DOI: 10.1103/physrevlett.126.210504. URL: http://dx.doi.org/10.1103/PhysRevLett.126.210504.

[67] Kazumi Okuyama. *Matter correlators through a wormhole in double-scaled SYK*. 2024. arXiv: 2312.00880 [hep-th]. URL: https://arxiv.org/abs/2312.00880.

[68] Don N. Page. "Information in black hole radiation". In: *Phys. Rev. Lett.* 71 (23 Dec. 1993), pp. 3743–3746. DOI: 10.1103/PhysRevLett.71.3743. URL: https://link.aps.org/doi/10.1103/PhysRevLett.71.3743.

[69] Geoffrey Penington. *Entanglement Wedge Reconstruction and the Information Paradox*. 2020. arXiv: 1905.08255 [hep-th]. URL: https://arxiv.org/abs/1905.08255.

[70] Joseph Polchinski and Vladimir Rosenhaus. "The spectrum in the Sachdev-Ye-Kitaev model". In: *Journal of High Energy Physics* 2016.4 (Apr. 2016), pp. 1–25. ISSN: 1029-8479. DOI: 10.1007/jhep04(2016)001. URL: http://dx.doi.org/10.1007/JHEP04(2016)001.

[71] Xiao-Liang Qi and Alexandre Streicher. "Quantum epidemiology: operator growth, thermal effects, and SYK". In: *Journal of High Energy Physics* 2019.8 (Aug. 2019). ISSN: 1029-8479. DOI: 10.1007/jhep08(2019)012. URL: http://dx.doi.org/10.1007/JHEP08(2019)012.

[72] Observables in Quantum Gravity: From Theory to Experiment. *Aspen Center for Physics Winter Conference*. 2025. URL: https://indico.global/event/1376/.

[73] E. Rabinovici et al. *A bulk manifestation of Krylov complexity*. 2023. arXiv: 2305.04355 [hep-th]. URL: https://arxiv.org/abs/2305.04355.

[74] Eliezer Rabinovici et al. *Krylov Complexity*. 2025. arXiv: 2507.06286 [hep-th]. URL: https://arxiv.org/abs/2507.06286.

[75] Daniel A. Roberts and Beni Yoshida. "Chaos and complexity by design". In: *Journal of High Energy Physics* 2017.4 (Apr. 2017). ISSN: 1029-8479. DOI: 10.1007/jhep04(2017)121. URL: http://dx.doi.org/10.1007/JHEP04(2017)121.

[76] Subir Sachdev and Jinwu Ye. "Gapless spin-fluid ground state in a random quantum Heisenberg magnet". In: *Physical Review Letters* 70.21 (May 1993), pp. 3339–3342. ISSN: 0031-9007. DOI: 10.1103/physrevlett.70.3339. URL: http://dx.doi.org/10.1103/PhysRevLett.70.3339.

[77] Gabor Sarosi. "AdS_2 holography and the SYK model". In: *Proceedings of XIII Modave Summer School in Mathematical Physics — PoS(Modave2017)*. Modave2017. Sissa Medialab, Mar. 2018. DOI: 10.22323/1.323.0001. URL: http://dx.doi.org/10.22323/1.323.0001.

[78] Yasuhiro Sekino and L Susskind. "Fast scramblers". In: *Journal of High Energy Physics* 2008.10 (Oct. 2008), pp. 065–065. ISSN: 1029-8479. DOI: 10.1088/1126-6708/2008/10/065. URL: http://dx.doi.org/10.1088/1126-6708/2008/10/065.

[79] Douglas Stanford. *More quantum noise from wormholes*. 2020. arXiv: 2008.08570 [hep-th]. URL: https://arxiv.org/abs/2008.08570.

[80] Kaixiang Su, Pengfei Zhang, and Hui Zhai. "Page curve from non-Markovianity". In: *Journal of High Energy Physics* 2021.6 (June 2021). ISSN: 1029-8479. DOI: 10.1007/jhep06(2021)156. URL: http://dx.doi.org/10.1007/JHEP06(2021)156.

[81] Brian Swingle et al. "Measuring the scrambling of quantum information". In: *Physical Review A* 94.4 (Oct. 2016). ISSN: 2469-9934. DOI: 10.1103/physreva.94.040302. URL: http://dx.doi.org/10.1103/PhysRevA.94.040302.

[82] C. Teitelboim. "Gravitation and Hamiltonian Structure in Two Space-Time Dimensions". In: *Phys. Lett. B* 126 (1983), pp. 41–45. DOI: 10.1016/0370-2693(83)90012-6.

[83] Akram Touil and Sebastian Deffner. "Information scrambling —A quantum thermodynamic perspective". In: *Europhysics Letters* 146.4 (May 2024), p. 48001. ISSN: 1286-4854. DOI: 10.1209/0295-5075/ad4413. URL: http://dx.doi.org/10.1209/0295-5075/ad4413.

[84] Vinay Tripathi et al. "Qudit Dynamical Decoupling on a Superconducting Quantum Processor". In: *Physical Review Letters* 134.5 (Feb. 2025). ISSN: 1079-7114. DOI: 10.1103/physrevlett.134.050601. URL: http://dx.doi.org/10.1103/PhysRevLett.134.050601.

[85] Philipp Uhrich et al. *A cavity quantum electrodynamics implementation of the Sachdev–Ye–Kitaev model*. 2023. arXiv: 2303.11343 [quant-ph]. URL: https://arxiv.org/abs/2303.11343.

[86] W. G. Unruh. "Notes on black-hole evaporation". In: *Phys. Rev. D* 14 (4 Aug. 1976), pp. 870–892. DOI: 10.1103/PhysRevD.14.870. URL: https://link.aps.org/doi/10.1103/PhysRevD.14.870.

[87] D.F. Walls and Gerard J. Milburn. "Input–Output Formulation of Optical Cavities". In: *Quantum Optics*. Ed. by D.F. Walls and Gerard J. Milburn. Berlin, Heidelberg: Springer Berlin Heidelberg, 2008, pp. 127–141. ISBN: 978-3-540-28574-8. DOI: 10.1007/978-3-540-28574-8_7. URL: https://doi.org/10.1007/978-3-540-28574-8_7.

[88] Shenglong Xu and Brian Swingle. "Scrambling Dynamics and Out-of-Time-Ordered Correlators in Quantum Many-Body Systems". In: *PRX Quantum* 5.1 (Jan. 2024). ISSN: 2691-3399. DOI: 10.1103/prxquantum.5.010201. URL: http://dx.doi.org/10.1103/PRXQuantum.5.010201.

[89] Norman Y. Yao et al. *Interferometric Approach to Probing Fast Scrambling*. 2016. arXiv: 1607.01801 [quant-ph]. URL: https://arxiv.org/abs/1607.01801.

[90] Beni Yoshida and Alexei Kitaev. *Efficient decoding for the Hayden-Preskill protocol*. 2017. arXiv: 1710.03363 [hep-th]. URL: https://arxiv.org/abs/1710.03363.

[91] Beni Yoshida and Norman Y. Yao. "Disentangling Scrambling and Decoherence via Quantum Teleportation". In: *Phys. Rev. X* 9 (1 Jan. 2019), p. 011006. DOI: 10.1103/PhysRevX.9.011006. URL: https://link.aps.org/doi/10.1103/PhysRevX.9.011006.

[92] Yi-Neng Zhou, Robin Löwenberg, and Julian Sonner. *Measuring Rényi entropy using a projected Loschmidt echo*. 2025. arXiv: 2504.05237 [quant-ph]. URL: https://arxiv.org/abs/2504.05237.